The testis protein ZNF165 is a SMAD3 cofactor that coordinates oncogenic TGFβ signaling in triple-negative breast cancer

Zane A. Gibbs[1,2], Luis C. Reza[1,2], Chun-Chun Cheng[1,2], Jill M. Westcott[3], Kathleen McGlynn[1,2], Angelique W. Whitehurst[1,2,*]

[1] Department of Pharmacology, University of Texas Southwestern Medical Center, Dallas, TX, 75390, USA

[2] Harold C. Simmons Comprehensive Cancer Center, University of Texas Southwestern Medical Center, Dallas, TX, 75390, USA

[3] Hamon Center for Therapeutic Oncology Research, University of Texas Southwestern Medical Center, Dallas, TX, 75390, USA

* To whom correspondence should be addressed. Tel: +1 2146456066; Email: angelique.whitehurst@utsouthwestern.edu

ABSTRACT

Cancer/testis (CT) antigens are proteins whose expression is normally restricted to germ cells yet aberrantly activated in tumors, where their functions remain relatively cryptic. Here we report that ZNF165, a CT antigen frequently expressed in triple-negative breast cancer (TNBC), associates with SMAD3 to modulate transcription of transforming growth factor β (TGFβ)-dependent genes and thereby promote growth and survival. In addition, we identify the KRAB zinc finger protein, ZNF446, and its associated tripartite motif protein, TRIM27, as obligate components of the ZNF165-SMAD3 complex that also support tumor cell viability. Importantly, we find that TRIM27 alone is necessary for ZNF165 transcriptional activity and is required for orthotopic tumor growth *in vivo*. Our findings indicate that aberrant expression of a testis-specific transcription factor is sufficient to co-opt somatic transcriptional machinery to drive a pro-tumorigenic gene expression program.

INTRODUCTION

Tumors frequently activate genes whose expression is normally restricted to the testes (Sahin et al. 2000; Atanackovic et al. 2007; Wang et al. 2016). Since the testes are immune-

31 privileged, the protein products encoded by these genes can evoke an immune response
32 when expressed in tumors (van der Bruggen et al. 1991; Sahin et al. 1995; Fijak and
33 Meinhardt 2006). Given this feature, these ~270 genes are collectively termed cancer/testis
34 (CT) genes and their encoded proteins are known as CT antigens (Simpson et al. 2005). CT
35 antigens have long been considered attractive targets for immunotherapy in a wide variety of
36 cancers (Whitehurst 2014; Thomas et al. 2018). In addition, recent work from multiple
37 groups has found that many CT antigens can support neoplastic behaviors in tumor cells
38 (Gibbs and Whitehurst 2018). Specifically, CT antigens have been implicated in supporting
39 mitotic progression, degradation of tumor suppressors, promoting DNA repair and thwarting
40 apoptosis (Whitehurst et al. 2010; Hosoya et al. 2011; Cappell et al. 2012; Maxfield et al.
41 2015; Pineda et al. 2015; Viphakone et al. 2015; Nichols et al. 2018; Gallegos et al. 2019).
42 Collectively, studies on CT antigen function over the last 15 years indicate that these
43 proteins are not merely innocuous by-products of aberrant tumor gene expression programs,
44 but rather integral agents of tumor growth and survival.
45 Using a large-scale, loss-of-function screening approach, our group previously identified
46 the CT antigen, ZNF165, as essential for triple-negative breast cancer (TNBC) survival
47 (Maxfield et al. 2015). Depletion of ZNF165 *in vitro* or *in vivo* reduces survival of TNBC cells.
48 Importantly, elevated ZNF165 mRNA expression correlates significantly with reduced
49 survival time in breast cancer, indicating that expression of this protein may confer an
50 aggressive tumorigenic phenotype (Maxfield et al. 2015).
51 ZNF165 is a C_2H_2 zinc finger transcription factor that contains an N-terminal SCAN
52 domain and six canonical Zn^{2+} fingers at its C-terminus. Consistent with its characterization
53 as a CT antigen, ZNF165 expression is restricted to human testes and is extremely low or
54 undetectable in normal breast tissues (Tirosvoutis et al. 1995; Maxfield et al. 2015).
55 Unfortunately, ZNF165 lacks conservation in mice, thereby precluding genetic studies that
56 could illuminate its normal function within the testes (Tirosvoutis et al. 1995). However,
57 investigation of its function in TNBC revealed that ZNF165 associates with chromatin to

58 regulate expression of its target genes, which includes approximately 25% of all TGFβ-
59 responsive genes in TNBC cells (Maxfield et al. 2015).
60 The cellular response to TGFβ is highly context selective, often resulting in dramatically
61 different phenotypes. For example, TGFβ is well known to facilitate growth inhibition in
62 breast epithelia and most other somatic tissues, primarily through transcriptional activation of
63 cyclin-dependent kinase inhibitors that result in cell cycle arrest (Hannon and Beach 1994;
64 Polyak et al. 1994; Morikawa et al. 2016). Conversely, TGFβ has also been shown to
65 stimulate the growth and differentiation of multiple cell types, including chondrocytes,
66 hematopoietic stem cells, and endothelial cells (Goumans et al. 2002; Li et al. 2005; Challen
67 et al. 2010). These contrasting responses to TGFβ are generally dictated by cell type-
68 specific transcription factors, which associate with TGFβ-responsive SMAD proteins
69 (SMAD3 and SMAD4) and recruit them to appropriate target genes for transcriptional
70 regulation (Chen et al. 2002; Gomis et al. 2006; Mullen et al. 2011; Massague 2012). In
71 TNBC, TGFβ induces a metastatic phenotype by promoting survival, chemoresistance, and
72 the epithelial-to-mesenchymal transition (Massague 2008; Bhola et al. 2013). These
73 processes are generally attributed to the activity of SMAD3, which binds directly to
74 chromatin, typically in complex with SMAD4. Notably, SMAD3 expression is elevated in late-
75 stage breast tumors compared to other receptor-activated SMADs (Tian et al. 2003; Padua
76 et al. 2008; Petersen et al. 2010).
77 Here, we investigate the mechanisms by which ZNF165 modulates TGFβ-dependent
78 transcription in TNBC. We find that ZNF165 co-occupies a subset of SMAD3 genomic
79 binding sites and physically interacts with SMAD3 on chromatin, enhancing SMAD3
80 recruitment to specific loci. We also identify ZNF446 and TRIM27, two proteins never
81 implicated in TGFβ signaling or TNBC, as critical components of the ZNF165-SMAD3
82 transcriptional complex. Importantly, loss of function of this complex, through genetic
83 inhibition of TRIM27, attenuates growth of an orthotopic xenograft model of TNBC *in vivo*.
84 These findings establish that anomalous expression of ZNF165 promotes the assembly of a

85 neomorphic transcriptional complex that contributes to oncogenic TGFβ transcription in
86 TNBC.
87
88 **RESULTS**
89 **SMAD3 is enriched at ZNF165 binding sites in TNBC cells**
90 To comprehensively investigate whether ZNF165 interfaces with the TGFβ transcriptional
91 network, we first generated a SMAD3 genomic binding profile in WHIM12 cells, where
92 ZNF165 is essential for growth (Maxfield et al. 2015). WHIM12 cells were originally
93 developed from a patient-derived xenograft established from a triple-negative, highly chemo-
94 resistant tumor (Li et al. 2013). Moreover, these cells are classified within the claudin-low
95 molecular subtype of breast cancer, which exhibits activated TGFβ signaling (Prat et al.
96 2010; Asiedu et al. 2011; Sabatier et al. 2014). We found that SMAD3 binding is associated
97 with over >27,000 sites in WHIM12 cells, comparable to previous studies of SMAD3 binding
98 in TNBC cell lines (Tufegdzic Vidakovic et al. 2015). Intersecting SMAD3 and ZNF165-
99 associated genes revealed that >90% of ZNF165 target genes are also bound by SMAD3,
100 an overlap representing a statistically significant enrichment ($p = 5.50e-120$, hypergeometric
101 distribution) (Figure 1A). This is in agreement with our previous findings that ZNF165 targets
102 a significant fraction of the TGFβ-responsive transcriptome (Maxfield et al. 2015). Mapping
103 the distance between binding sites further revealed that 90% of shared targets were bound
104 by both transcription factors at a distance of less than 100 kb from one another (Figure 1B).
105 Furthermore, 36% of shared target genes had ZNF165 and SMAD3 binding sites within 1 kb,
106 a proximity at which both factors exhibited overlap on chromatin due to the broad enrichment
107 profile of SMAD3 as observed within our dataset (Figure 1B-E). We next established
108 ZNF165 and SMAD3 binding profiles in SUM159 cells, which are also classified within the
109 claudin-low molecular subtype and require ZNF165 for viability (Prat et al. 2010; Maxfield et
110 al. 2015). SMAD3 enrichment at the ZNF165 binding sites here closely resembled that of
111 WHIM12 cells (Figure 1C-E). Further analysis of SMAD3 binding in MDA-MB-231 cells

112 corroborated these findings (Figure 1-figure supplement 1A-C). Together these data
113 demonstrate that despite differences in the genetic backgrounds of TNBC tumor cells,
114 ZNF165 and SMAD3 exhibit significant co-occupancy on chromatin throughout the genome.
115 We next applied a motif discovery strategy to the 118 regions where both transcription
116 factors were bound within 1 kb of each other. More than 50% of these co-bound sites were
117 present in gene promoters (-1 kb or +100 base pairs from TSS) while SMAD3 binding sites
118 were relatively evenly distributed across genetic regions (Figure 1F). This analysis revealed
119 that GC-rich elements are significantly enriched at co-bound regions (n=118) compared to
120 those bound by ZNF165 alone (n=204) (Figure 1G and 1H). Such GC-rich SMAD binding
121 elements (SBEs) have recently been characterized as universal binding sites for receptor-
122 activated SMAD proteins, and SMAD3 can bind variants of these motifs with high affinity
123 (Martin-Malpartida et al. 2017). Thus, the GC-rich SMAD3 binding element may be an
124 underlying genomic feature of the ZNF165-occupied sites that facilitates co-occupancy.
125 Collectively, these data suggest that ZNF165 and SMAD3 may form cis-regulatory modules
126 on chromatin to direct TGFβ-mediated gene expression in TNBC. In support of this notion,
127 gene set enrichment analysis of ZNF165-responsive genes in WHIM12 cells revealed a
128 significant enrichment of genes involved in the epithelial-to-mesenchymal transition (EMT), a
129 SMAD3-dependent process that promotes metastasis in response to TGFβ signaling (Figure
130 1-figure supplement 1D) (Tian et al. 2003; Xu et al. 2009; Petersen et al. 2010). Consistent
131 with this, elevated ZNF165 expression in patients with breast cancer is associated with a
132 greater metastatic potential (Hazard Ratio (HR) = 1.4; p = 0.004) (Figure 1-figure
133 supplement 1E).
134
135 **ZNF165 and SMAD3 cooperate to modulate TGFβ-responsive gene expression**
136 Given the enrichment of SMAD3 and ZNF165 at shared sites and their general proximity to
137 one another on chromatin, we next asked whether these transcription factors cooperate to
138 regulate expression of co-bound genes. We leveraged a previously generated gene

139 expression data set of TGFβ responsiveness in WHIM12 cells (Maxfield et al. 2015). Here,
140 we assembled a set of 65 TGFβ-responsive genes that are co-bound by SMAD3 and
141 ZNF165 (Figure 2-figure supplement 1A). We then compared the impacts of ZNF165 and
142 SMAD3 depletion on a subset of these genes. This analysis revealed a significant correlation
143 (r = 0.52) between expression fold-changes in response to depletion of either transcription
144 factor (Figure 2A). In particular, ZNF165 and SMAD3 were required to either activate or
145 repress expression of the majority of shared target genes (quadrant I and III, Figure 2A). We
146 also observed opposing effects of SMAD3 and ZNF165 on a smaller subset of genes,
147 suggesting that in some cases, the activities of these two proteins may oppose one another
148 (quadrant II and quadrant IV, Figure 2A).
149 The observed expression changes in Figure 2A suggest two modes of regulation for
150 ZNF165-SMAD3 targets. First, ZNF165 collaborates with SMAD3 to activate or oppose
151 TGFβ-mediated gene expression changes (quadrant I and III, Figure 2A). Alternatively,
152 ZNF165 can antagonize SMAD3-mediated activation or repression of shared target genes in
153 response to TGFβ (quadrant II and IV, Figure 2A). The majority of genes fell into the former
154 category, with *SMURF2* and *RRAD* being the two most responsive and were thus selected
155 as archetypes for follow-up analysis. Importantly, we found that RRAD and SMURF2 protein
156 accumulation corresponded to mRNA alterations upon ZNF165 or SMAD3 depletion (Figure
157 2B and 2C).
158 Given the observed collaborative function of ZNF165 and SMAD3 on target gene
159 expression, we next asked whether their association with chromatin was cooperative.
160 ZNF165 knockdown resulted in a ~50% reduction of SMAD3 enrichment at the ZNF165
161 binding sites proximal to both *SMURF2* and *RRAD* (Figure 2D). Importantly, SMAD3 binding
162 at the promoter of LBH, a site not co-bound by ZNF165, was unaffected by ZNF165
163 depletion. SMAD3 commonly recruits the histone acetyltransferase, p300, to activate gene
164 expression of its targets (Feng et al. 1998; Janknecht et al. 1998). Consistent with this, we
165 observed a reduction of H3K27ac at the ZNF165-SMAD3 binding site proximal to *RRAD* in

166 response to ZNF165 knockdown (Figure 2E). Conversely, an increase in H3K27ac was
167 detected upon ZNF165 overexpression (Figure 2F). These findings suggest that ZNF165 is
168 essential for recruitment of SMAD3 to shared target gene promoters and transcriptional
169 activation. We reasoned that this activity could promote expression of genes required for
170 tumorigenic phenotypes. Indeed, a report from 2001 indicated that RRAD is sufficient to
171 promote proliferation of breast tumor cells *in vitro* and *in vivo* (Tseng et al. 2001). Based on
172 this observation, we investigated breast cancer gene expression data sets for clinical
173 correlates with RRAD expression. In the mesenchymal subtype of TNBC, which is enriched
174 for active TGFβ signaling and an EMT gene expression signature, RRAD expression
175 correlated with reduced overall survival (HR = 2.31; p = 0.04) and greater metastatic
176 potential (HR = 3.18; p = 0.05) (Figure 2-figure supplement 1B) (Lehmann et al. 2011).
177 Conversely, in luminal tumors, which are traditionally ER^+ and exhibit tumor-suppressive
178 TGFβ signaling, RRAD expression correlated with improved overall survival (HR = 0.63; p =
179 0.01) and no correlation was observed with distant metastasis free survival (HR = 1.12; p =
180 0.55) (Figure 2-figure supplement 1C) (Perou et al. 2000; Sato et al. 2014). Moreover,
181 DepMap analysis revealed that RRAD perturbation generally leads to a reduction in 2D
182 growth of TNBC cell lines, and we found that RRAD was essential for growth of SUM159
183 cells in soft agar (Figure 2-figure supplement 1D and 1E). However, we observed an
184 enhanced growth phenotype in ER^+ MCF7 cells, supporting the notion that TGFβ mediates
185 tumor-suppressive phenotypes in more differentiated breast cancer cells and pro-
186 tumorigenic effects in less differentiated cell types (Figure 2-figure supplement 1F) (Tian et
187 al. 2003; Massague 2008). Collectively, these data suggest that ZNF165 is capable of
188 directing SMAD3 recruitment to TGFβ-responsive target genes, whose altered expression
189 can support malignant behaviors in the context of TNBC.
190
191 **ZNF165 physically associates with SMAD3 in a TGFβ-dependent manner**

192 As ZNF165 appears to facilitate SMAD3 recruitment to chromatin, we asked whether these
193 proteins physically associate. Interaction studies using co-expression/co-
194 immunoprecipitation indicated an association between ZNF165 and SMAD3 (Figure 3A). In
195 addition, we found that ZNF165 interacts with the active, phosphorylated form of SMAD3 on
196 chromatin in SUM159 cells stably expressing ZNF165-V5 (Figure 3B). Activation of SMAD3
197 and its resulting nuclear translocation is dependent on the phosphorylation of its C-terminus
198 by TGFβRI in response to TGFβ (Massague 2012). Thus, we employed the serine/threonine
199 kinase inhibitor SB-431542, which selectively inhibits TGFβRI and downstream
200 phosphorylation of SMAD3, to assess whether the ZNF165-SMAD3 interaction is dependent
201 on pathway activation (Figure 3C) (Inman et al. 2002; Massague 2012). Proximity ligation
202 assays (PLAs) in SUM159 cells treated with TGFβ revealed an endogenous association
203 between ZNF165 and SMAD3, which was significantly diminished by pre-treatment with SB-
204 431542 (Figure 3D). Furthermore, we found that endogenous ZNF165 and SMAD4 also
205 interact in a TGFβ-dependent manner (Figure 3E). Taken together, these results indicate
206 that in response to TGFβ, ZNF165 physically associates with phosphorylated SMAD3.
207
208 **ZNF446 is an obligate component of the ZNF165-SMAD3 transcriptional complex**
209 We reasoned that ZNF165 and SMAD3 likely function within a multi-protein transcriptional
210 complex to mediate gene expression changes in response to TGFβ. Therefore, we searched
211 for additional ZNF165 interactors using proteomics data generated from a systematic yeast
212 two-hybrid (Y2H) screening approach (Rolland et al. 2014). This search returned 48 putative
213 ZNF165 interacting partners, 17 of which are likely transcriptional regulators based on the
214 presence of known gene regulatory domains (Supplementary File 2). To triage these
215 candidates, we focused on those containing a SCAN (SRE-ZBP, Ctfin51, AW-1 and Number
216 18) domain, which is well-documented to mediate specific interactions among SCAN-zinc
217 finger proteins (ZFPs) and the only domain within ZNF165 aside from its zinc finger array
218 (Figure 4A) (Edelstein and Collins 2005). We identified five putative interactors with SCAN

219 domains and examined the consequences of their depletion on *SMURF2* expression. Of the
220 proteins tested, ZNF446 and SCAND1 phenocopied the changes in gene expression
221 observed for ZNF165 and SMAD3 in two TNBC cell lines (Figure 4B). Examination of their
222 tumor expression patterns revealed that ZNF446 is upregulated in breast tumors, an
223 increase that trends with reduced survival in the triple-negative enriched basal-like subtype
224 of breast cancer (HR = 1.89; p = 0.059) (Figure 4-figure supplement 1A and 1B) (Perou et al.
225 2000; Sorlie et al. 2001). Moreover, we found that depletion of ZNF446 significantly reduced
226 anchorage-independent growth of TNBC cells (Figure 4-figure supplement 1C). Co-
227 expression/co-immunoprecipitation assays confirmed that ZNF165 and ZNF446 interact and
228 that deletion of the ZNF165 SCAN domain abrogates this association (Figure 4C). In
229 addition, an endogenous interaction between ZNF165 and ZNF446 was detectable in TNBC
230 tumor cell nuclear extracts, confirming these proteins interact in the relevant subcellular
231 compartment (Figure 4D). We then employed the SMAD3/4 PLA assay described above and
232 found that ZNF446 interacts with both SMAD3 and SMAD4 in a TGFβ-dependent fashion,
233 similar to ZNF165 (Figure 4E and 4F).
234 To determine if ZNF446 also associates with ZNF165-SMAD3 target genes, we
235 performed ChIP-seq for ZNF446-V5 stably expressed in WHIM12 and SUM159 cells. This
236 led to the identification of 5,039 and 7,926 binding sites in WHIM12 and SUM159 cells,
237 respectively. In both cell lines, ZNF446 was enriched at the ZNF165 binding sites (Figure 5A
238 and 5B; Figure 5-figure supplement 1A). Intersecting the ZNF446 and ZNF165 genomic
239 binding profiles further revealed a highly statistically significant overlap in both settings (p =
240 <0.0001) (Figure 5C and 5D). Approximately half of all ZNF446 binding sites in WHIM12
241 cells were also co-occupied by SMAD3 (Figure 5E and 5F; Figure 5-figure supplement 1B).
242 These co-bound sites were largely enriched for promoter regions compared to the total
243 binding sites for either factor (Figure 5-figure supplement 1C). Of further significance,
244 differential motif enrichment analysis revealed the presence of a short GC-rich element at
245 ZNF446-SMAD3 bound sites, closely resembling the motif we identified at ZNF165-SMAD3

246 bound sites and identical to the recently reported SMAD consensus binding motif (Figure 5G
247 and 5H; Figure 1G) (Martin-Malpartida et al. 2017).
248 With respect to target genes, we found that over half of those shared by ZNF165 and
249 SMAD3 (251/446) are also targeted by ZNF446 (Figure 5I). The impact of ZNF446 depletion
250 on expression of these genes significantly correlated with both ZNF165 (r = 0.49) and
251 SMAD3 (r = 0.86) (Figure 5J). Collectively, these findings implicate ZNF446 as a member of
252 the ZNF165-SMAD3 complex that can influence TGFβ-dependent transcription in TNBC.
253
254 **TRIM27 is essential for ZNF165 transcriptional activity and tumor growth *in vivo***
255 ZNF446 contains a KRAB (Krüppel-associated box) domain, which is well documented to
256 interact with the RBCC (RING, B-box, coiled-coil) domain of proteins within the tripartite
257 motif (TRIM) family that in turn function as co-repressors or, as recently demonstrated, co-
258 activators (Friedman et al. 1996; Schultz et al. 2001; Schultz et al. 2002; Chen et al. 2019).
259 Y2H-based proteomics confirmed such an interaction of TRIM27, which contains the classic
260 RBCC domain, with ZNF446 (Figure 6A; Supplementary File 2). Originally identified as an
261 oncogenic fusion with the RET tyrosine kinase, TRIM27 has been ascribed roles in
262 numerous cellular processes that include transcriptional repression, proliferation, meiosis,
263 innate immunity, and endosomal trafficking (Takahashi et al. 1985; Shimono et al. 2000;
264 Shimono et al. 2003; Zha et al. 2006; Hao et al. 2013; Zaman et al. 2013; Zheng et al. 2015;
265 Ma et al. 2016). However, its function as a transcriptional regulator in TNBC has not been
266 characterized. Co-expression/co-immunoprecipitation experiments revealed that both
267 ZNF446 and ZNF165 interact with TRIM27 and that all three proteins immunoprecipitate as
268 a complex (Figure 6B). We subsequently confirmed a nuclear interaction between ZNF165-
269 V5 and endogenous TRIM27 by proximity ligation in SUM159 cells and found that TRIM27
270 depletion also phenocopied changes in ZNF165-SMAD3 target gene expression (r = 0.81)
271 (Figure 6C and 6D). Notably, TRIM27 appears to be bi-functional, either positively or
272 negatively regulating expression of the ZNF165-SMAD3 targets (Figure 6D). Indicative of a

273 co-activator function, we found that TRIM27 is required for the transcriptional activation of
274 *RRAD* following ZNF165 or ZNF446 overexpression (Figure 6E; Figure 6-figure supplement
275 1A). Similar to ZNF165 and ZNF446, proximity ligation assays revealed endogenous,
276 nuclear interactions between TRIM27 and both SMAD3 and SMAD4, which were reduced by
277 TGFβ pathway inhibition (Figure 6F and 6G).

278 TRIM27 expression is elevated in several cancers including colon, lung, endometrial and
279 ovarian, and often correlates with poor prognosis (Tsukamoto et al. 2009; Horio et al. 2012;
280 Iwakoshi et al. 2012; Zoumpoulidou et al. 2012; Ma et al. 2016; Zhang et al. 2018). Using
281 TCGA data, we found that TRIM27 expression is significantly elevated in TNBC compared to
282 normal breast tissue (Figure 6-figure supplement 1B). Moreover, we stained a small cohort
283 of normal and TNBC tissues for TRIM27 and observed a striking difference in its subcellular
284 localization. TRIM27 appeared to be predominantly cytoplasmic in normal breast epithelia
285 and more nuclear in TNBC tissues, suggesting that its transcriptional activity might associate
286 with the transformed state (Figure 6-figure supplement 1C). This finding is in agreement with
287 previous reports and the Human Tissue Atlas, where TRIM27 is mostly cytoplasmic in
288 normal breast and nuclear in testis and a subset of breast cancer tissues (Tezel et al. 1999;
289 Tezel et al. 2009; Uhlen et al. 2015).

290 Given that TRIM27 was critical for ZNF165-dependent gene regulation, we next asked
291 whether TRIM27 was essential for malignant behaviors. While depletion of TRIM27 does not
292 seem to strongly affect TNBC tumor cell growth in 2D, we observed a significant defect in
293 anchorage-independent growth using soft agar assays (Figure 6-figure supplement 1D and
294 1E). We next perturbed TRIM27 as a means to inhibit the activity of the ZNF165
295 transcriptional complex and assess its impact on TNBC tumor growth and survival at the
296 orthotopic site in mice. Following stable depletion of TRIM27, SUM159 cells were injected
297 into the mammary fat pad of immunocompromised mice (Figure 6-figure supplement 1F and
298 1G). We observed a significant decrease in tumor size, suggesting that TRIM27 is essential
299 for TNBC tumor growth *in vivo* and that inhibition of the ZNF165 transcriptional complex may

300 be a promising avenue of therapeutic intervention (Figure 6H and 6I). Together, these
301 results indicate that TRIM27 is a previously unrecognized regulatory component of TGFβ
302 signaling in TNBC and functions to modulate TGFβ-dependent transcription in cooperation
303 with ZNF165, ZNF446, and SMAD3.
304
305 **DISCUSSION**
306 Striking similarities between tumors and developing germ cells have been noted for over a
307 century (Simpson et al. 2005). As a result, it has been speculated that a fundamental
308 attribute of cancer is the usurpation of developmental signaling programs. Tumors frequently
309 activate expression of gametogenic genes, which encode a group of proteins termed
310 cancer/testis antigens (CT antigens) (Chen et al. 1997; Simpson et al. 2005). While these
311 proteins have long been considered optimal targets for immunotherapy, their function, if any,
312 in tumor cells has not been well-established.
313 In recent years, an increasing number of studies have begun to indicate that CT antigens
314 are not merely innocuous by-products of aberrant gene expression programs, but instead
315 can be essential to the progression of cancer. The list of tumor cell mechanisms regulated
316 by these proteins includes mitosis, protein turnover, mitigating DNA damage, and disrupting
317 normal transcriptional programs (Gibbs and Whitehurst 2018). This variety of biological
318 processes is attributable to the high degree of diversity in the functions of proteins classified
319 as CT antigens, and speaks to the ability of tumor cells to engage aberrant gene expression
320 programs in order to support their growth and survival. In support of this, our study of the
321 testis protein ZNF165 has revealed a previously unrecognized mechanism by which TGFβ
322 signaling is co-opted to promote malignancy in late-stage breast tumors.
323 Our findings expose a high degree of flexibility in tumor cell transcriptional networks. We
324 reason that this feature could be the result of the modular domains present in many
325 transcriptional regulators, particularly zinc finger proteins (ZFPs), which make up the largest
326 family of transcription factors in the human genome (Lambert et al. 2018). The vast majority

327 of these proteins contain KRAB, BTB/POZ, or SCAN domains, that mediate interactions with
328 transcriptional partners (Bellefroid et al. 1991; Bardwell and Treisman 1994; Albagli et al.
329 1995; Williams et al. 1995). The SCAN domain in particular regulates the assembly and thus
330 function of specific transcriptional complexes (Edelstein and Collins 2005). SCAN domains
331 are not promiscuous, but demonstrate selectivity for co-association, the basis of which is not
332 clear. Nevertheless, ectopic introduction of a SCAN domain-containing protein, such as
333 ZNF165, may drive assembly of a neomorphic transcriptional complex, ZNF165-ZNF446-
334 SMAD3-TRIM27, that is otherwise not present in somatic cells (Figure 7). This finding
335 highlights the importance of silencing lineage-specific transcription factors, as their
336 anomalous expression may be sufficient to disrupt transcriptional networks that regulate
337 tissue homeostasis.

338 The study of CT antigen function generally, and ZNF165 in particular, has the capacity to
339 reveal new principles underlying tumor cell regulatory networks. Specifically, our data
340 indicate that both ZNF446 and TRIM27 are complicit in the activation of oncogenic TGFβ
341 signaling in TNBC. While ZNF446 has been reported to act as a transcriptional repressor for
342 SRF and AP-1 via its KRAB domain, a physiological function for ZNF446 in either normal or
343 malignant contexts has not been reported (Liu et al. 2005). Our findings suggest that in
344 addition to functioning as a chromatin-bound cofactor for ZNF165 and SMAD3, ZNF446 may
345 recruit TRIM27 to modulate TGFβ-induced transcription on a subset of targets. Furthermore,
346 despite reports describing only repressive capabilities of TRIM27, we find that TRIM27 can
347 either activate or repress expression of genes targeted by the ZNF165-ZNF446-SMAD3
348 complex (Shimono et al. 2000; Shimono et al. 2003). This finding dovetails with a recent
349 report demonstrating that TRIM28 serves as a co-activator for ZFP30-mediated
350 adipogenesis, and together these studies begin to establish that tripartite motif proteins may
351 be bi-functional with respect to transcriptional repression or activation (Chen et al. 2019).
352 TRIM27 is also a well characterized E3 ligase and has been reported to modify numerous
353 protein substrates via ubiquitination and SUMOylation (Chu and Yang 2011; Zurek et al.

354 2012; Lee et al. 2013). Future studies to address whether the catalytic activity of TRIM27 is
355 required for ZNF165-dependent transcriptional regulation are therefore crucial, as small
356 molecule inhibitors of TRIM27 could selectively disrupt pro-tumorigenic TGFβ signaling in
357 TNBC.

358 An additional, unexpected finding is that *RRAD*, whose transcription is highly regulated by
359 the ZNF165 transcriptional complex, is a TGFβ target gene that can exert opposing
360 behaviors depending on context. TGFβ signaling is well known to drive pro-tumorigenic
361 phenotypes in less differentiated breast tumor cell types, such as TNBC, while facilitating
362 tumor suppression in more differentiated cell types (Tian et al. 2003; Massague 2008). Our
363 study indicates that RRAD contributes to such context-specific phenotypes conferred by
364 TGFβ signaling, which may help to explain extensive data that report opposing impacts of
365 RRAD expression in a variety of cancer types (Suzuki et al. 2007; Lee et al. 2010; Mo et al.
366 2012; Yeom et al. 2012). With respect to function, RRAD is a small GTPase reported to
367 negatively regulate L-type calcium channels in the heart, where its deficiency can promote
368 cardiac hypertrophy (Chang et al. 2007; Manning et al. 2013; Meza et al. 2013). In cancer,
369 RRAD has been implicated in numerous processes, including the regulation of glycolysis,
370 proliferation, NF-κB signaling, and apoptosis (Lee et al. 2010; Yeom et al. 2012; Hsiao et al.
371 2014; Zhang et al. 2014; Liu et al. 2015; Shang et al. 2016). Although the exact function of
372 RRAD in TNBC will need to be elucidated in future studies, the vast array of phenotypes
373 associated with this protein undoubtedly reflect the context within which it functions.
374 Ultimately, further investigation could indicate that RRAD itself is a tractable intervention
375 point in TNBC.
376

377 **MATERIAL AND METHODS**

378 **Cell lines and transfections**

379 Cell lines were obtained from American Type Culture Collection (ATCC) except for: WHIM12
380 (Matthew Ellis, Baylor College of Medicine), SUM159 (Asterand), and SUM159T-Luceiferase

381 (Gray Pearson, Georgetown University). All cell lines were cultured in the provider's
382 recommended medium. For siRNA transfections, cells were trypsinized and seeded in Opti-
383 MEM™ containing Lipofectamine RNAiMAX (Thermo Fisher Scientific, Waltham, MA) and
384 pooled siRNAs at a final concentration of 50 nM. cDNA transfections in HEK293T cells were
385 performed using the calcium phosphate method as previously described (Maxfield et al.
386 2015).
387
388 **Antibodies and reagents**
389 The following antibodies were used for immunoblotting: HA (3F10; 1:1000; Roche, Basel,
390 Switzerland), c-Myc (sc-789; 1:1000; Santa Cruz Biotechnology; Dallas, TX), V5 (13202;
391 1:1000; Cell Signaling Technology, Danvers, MA), SMAD3 (ab28379; 1:1000; Abcam,
392 Cambridge, United Kingdom), phospho-SMAD3 (9520, 1:1000; Cell Signaling Technology),
393 SMURF2 (sc-393848; 1:500; Santa Cruz Biotechnology), RRAD (PA537885; 1:1000;
394 Thermo Fisher Scientific), ZNF165 (2B8; 1:1000; Novus Biologicals, Centennial, CO),
395 ZNF165 (HPA007247, 1:1000; Atlas Antibodies, Bromma, Sweden), Tubulin (2128; 1:1000;
396 Cell Signaling Technology), ZNF446 (16218-1-AP; 1:1000; Proteintech, Rosemont, IL),
397 TRIM27 (15099; 1:1000; Cell Signaling Technology). The following antibodies were used for
398 proximity ligation assays: V5 (R960-25; 1:500; Thermo Fisher Scientific), SMAD3 (ab28379;
399 1:200; Abcam), SMAD3 (sc-101154, 1:200; Santa Cruz Biotechnology), SMAD4 (sc-7966;
400 1:200, Santa Cruz Biotechnology), ZNF165 (HPA007247, 1:200; Atlas Antibodies), ZNF446
401 (16218-1-AP; 1:200; Proteintech), TRIM27 (12205-1-AP; 1:200, Proteintech). ChIP-qPCR
402 experiments were performed with 1.5 µg SMAD3 (ab28379; Abcam), 5 µg phospho-SMAD3
403 (9520; Cell Signaling Technology), 2 µg H3K27ac (ab4729; Abcam), or the appropriate
404 amount of normal rabbit IgG (2729; Cell Signaling Technology). ChIP-seq in WHIM12 and
405 SUM159 cells was performed with 10 µg SMAD3 (ab28379; Abcam) or 5 µg V5 (ab9116;
406 Abcam). Immunoprecipitations used for interaction studies were performed with HA (3F10;

407 Roche), V5 (R960-25; Thermo Fisher Scientific), and ZNF165 (HPA007247, 1:200; Atlas
408 Antibodies). IHC was performed using TRIM27 (12205-1-AP; Proteintech) at 1:200.
409 Transforming growth factor-β1 was purchased from Cell Signaling Technology (8915) and
410 SB-431542 was purchased from Tocris Bioscience (Bristol, United Kingdom) (1614). siRNAs
411 targeting ZNF165, SMAD3, ZNF446, TRIM27, SCAND1, ZNF24, ZNF263, or ZKSCAN8, and
412 non-targeting control #2 were obtained from Dharmacon (Lafayette, CO) (siGENOME
413 siRNA). siRNAs targeting RRAD (SASI_Hs01_00221658, SASI_Hs01_00221655,
414 SASI_Hs01_00221652, SASI_Hs01_00221653) and shRNAs targeting TRIM27 (SHCLNG-
415 NM_006510; TRCN0000280319 and TRCN0000011021) or a non-targeting control were
416 purchased from Sigma (St. Louis, MO).
417
418 **Expression plasmids**
419 ZNF165 and ZNF446 cDNA was purchased in pDONR223 vectors from the DNASU Plasmid
420 Repository (Tempe, AZ) and cloned into pLX302-V5 or pLX304-V5 lentiviral vectors,
421 respectively, using the Gateway™ Cloning system (Thermo Fisher Scientific). psPAX2 and
422 pMD2.G were gifts from Didier Trono (Addgene plasmids #12260 and #12259). SMAD3,
423 SMAD4, and TRIM27 cDNA was obtained in pENTR221 vectors from the UT Southwestern
424 (UTSW) McDermott Center for Human Genetics and subcloned into pCMV-HA or pCMV-
425 myc (Clontech, Mountain View, CA) between SalI and NotI restriction sites. pCMV6-ZNF165-
426 myc was obtained from Origene (Rockville, MD) (RC205600). The SCAN domain of pCMV6-
427 ZNF165-myc was deleted using overlap extension PCR and verified by sequencing and
428 western blot (primers listed in Supplementary File 1).
429
430 **Generation of stable cell lines**
431 Stable cell lines were generated through lentiviral-mediated transduction. HEK293T cells
432 were co-transfected with the target gene vectors (pLX302 or pLX304) and lentiviral
433 packaging plasmids (psPAX2 and pMD2.G). Virus conditioned media was collected 48h post

434 transfection and used to infect target cells in the presence of polybrene. Selection with
435 appropriate antibiotics was performed for 3 days following infection to generate stable
436 populations. ZNF165-V5 or ZNF446-V5 expression was confirmed by RT-qPCR, western
437 blotting, and immunofluorescence.
438
439 **Western blotting and gene expression analysis**
440 Western blotting was done as previously described (Maxfield et al. 2015). RNA was isolated
441 using the GenElute™ Mammalian Total RNA Miniprep Kit (Sigma), and 500 ng RNA was
442 reverse transcribed using the High Capacity cDNA Reverse Transcription Kit (Thermo Fisher
443 Scientific) according to manufacturer's instructions. Taqman Real-Time PCR (Thermo Fisher
444 Scientific) gene expression assays were run in technical duplicate to quantify expression on
445 an Applied Biosystems QuantStudio™ 5 Real-Time PCR System. Relative expression
446 values were calculated using the $2^{-\Delta\Delta CT}$ method and the data were normalized to RPL27
447 values. Catalog numbers for Taqman probes can be found in Supplementary File 1.
448
449 **Chromatin immunoprecipitation (ChIP) and sequencing (ChIP-seq)**
450 Cells were grown to ~90% confluency and crosslinked with 1% formaldehyde for 15 minutes
451 at 37°C. Crosslinking was then quenched with 0.125 M glycine for 5 minutes at 4°C. Cells
452 were washed twice with cold PBS and lysed in hypotonic buffer (5 mM PIPES pH 8, 85 mM
453 KCl, 0.5% NP-40, 1 mM DTT). All buffers were supplemented with Complete Protease
454 Inhibitor Cocktail (Sigma). Nuclei were pelleted at 2,000 rpm for 5 minutes and resuspended
455 in lysis buffer containing 50 mM Tris pH 7.9, 1% SDS, 10 mM EDTA, and 1 mM DTT.
456 Chromatin was sheared into 200-400 bp fragments using a Bioruptor sonicator (Diagenode),
457 clarified by centrifugation at max speed for 10 minutes, and diluted (1:10) in buffer containing
458 20 mM Tris pH 7.9, 0.5% Triton X-100, 150 mM NaCl, 2 mM EDTA, and 1 mM DTT. Lysates
459 were pre-cleared with Protein A/G agarose beads (Thermo Fisher Scientific) for 1 hour and,
460 following removal of input material, incubated with appropriate antibodies overnight at 4°C.

461 Protein A/G agarose beads blocked with BSA were then added to lysates for 2 hours,
462 followed by one low salt wash (20 mM Tris pH 7.9, 125 mM NaCl, 0.05% SDS, 1% Triton X-
463 100, 2 mM EDTA), one high salt wash (20 mM Tris pH 7.9, 500 mM NaCl, 0.05% SDS, 1%
464 Triton X-100, 2 mM EDTA), a more stringent wash (10 mM Tris pH 7.9, 250 mM LiCl, 1%
465 NP-40, 1% sodium deoxycholate, 1 mM EDTA), and a final wash in TE buffer (10 mM Tris
466 pH 7.9, 1 mM EDTA). For western blotting of immunoprecipitated proteins, beads were
467 boiled in 2X Laemmli sample buffer (containing 4% β-mercaptoethanol) for 5-10 minutes.
468 Otherwise, chromatin was eluted from beads with 100 mM NaHCO3 and 1% SDS, and de-
469 crosslinking was carried out overnight at 65°C. RNA and protein were digested with RNase
470 A (3 µg/mL) and Proteinase K (50 µg/mL), respectively. DNA was purified using
471 phenol/chloroform/isoamyl alcohol (25:24:1) and precipitated overnight with isopropyl alcohol
472 at -20°C.
473 Libraries of ChIP DNA were prepared using the KAPA Hyper Prep Kit (KAPA Biosystems,
474 Cape Town, South Africa) according to the manufacturer's instructions. Samples were
475 multiplexed with Illumina adapters (NEB, Ipswich, MA) and 75 bp single end reads (~50M
476 per sample) were generated on an Illumina NextSeq 500 (UTSW McDermott Center Next
477 Generation Sequencing Core). Raw reads were aligned to the human genome assembly
478 (hg19) using Bowtie2 (ver 2.3.2) with the "sensitive" parameters enabled, and the mapped
479 read files were sorted and indexed with SAMtools (ver 1.6). BigWig files for visualization on
480 the IGV genome browser (Robinson et al. 2011) were generated using DeepTools (ver
481 2.3.5). ChIP-seq was performed using biological duplicates for each sample. WHIM12
482 ZNF165-V5 ChIP-seq data was previously generated and is available under GEO accession
483 GSE65937. All other ChIP-seq datasets have been deposited under GEO accession
484 GSE130364.
485
486 **ChIP-seq peak calling and annotation**

487 Peaks were called using the HOMER (ver 4.9) findPeaks module with size and minimum
488 distance parameters set to 150 bp and 370 bp, respectively. Target genes for ZNF165,
489 SMAD3, and ZNF446 were defined for each transcription factor using GREAT version 3.0.0
490 (great.stanford.edu) with default parameters. The HOMER mergePeaks module was used to
491 identify overlapping peaks with a size parameter of 1000 bp. Tag density plots were
492 generated using the HOMER annotatePeaks module with size and bin size parameters set
493 to 5000 and 5 bp, respectively. The same module with the genomeOntology parameter
494 enabled was used to annotate the genomic regions associated with each factor. For
495 heatmap generation, the HOMER annotatePeaks module was used to create matrix files,
496 which were clustered with Cluster 3.0 and visualized with Java TreeView (ver 1.1.6r4). To
497 identify motifs enriched at co-bound sites, motif discovery was performed with MEME (ver
498 5.1.1) in "differential enrichment" mode. Motif density plots were generated using the
499 HOMER annotatePeaks module with size and bin size parameters set to 5000 and 5 bp,
500 respectively.
501
502 **ChIP-qPCR**
503 ChIP was performed as described above, and qPCR was carried out using SYBR green
504 reagents in technical duplicates (Thermo Fisher Scientific) on an ABI QuantStudio™ 5 Real-
505 Time PCR System. Three ten-fold dilutions were used to generate standard curves and the
506 amount of ChIP DNA relative to corresponding input values (percent input) was calculated.
507 SMAD3 enrichment was determined relative to IgG percent input values within the same
508 treatment or condition. Primer sequences are listed in Supplementary File 1.
509
510 **Proximity ligation assays**
511 Proximity ligation assays (PLAs) were performed using Duolink® reagents (Sigma)
512 according to manufacturer's instructions. Briefly, cells attached to glass coverslips were fixed
513 with 3.7% formaldehyde for 15 minutes and then permeabilized with 0.5% Triton X-100 for

514 15 minutes. Blocking was performed for 1 hour at 37°C, and cells were incubated with
515 appropriate antibodies overnight at 4°C. After washing, coverslips were incubated with PLUS
516 (rabbit) and MINUS (mouse) secondary probes for 1 hour at 37°C. Ligation was performed
517 for 30 minutes at 37°C, followed by rolling circle amplification for 100 minutes at 37°C.
518 Coverslips were washed, mounted to glass slides in medium containing DAPI, and kept at
519 4°C. Cells were imaged using a Keyence BZ-X710 fluorescence microscope at 100x
520 magnification and 5-10 regions of interest were captured on each coverslip. PLA signals
521 were quantified using ImageJ by counting the average number of foci per nucleus in any
522 given image.
523
524 **Immunoprecipitation**
525 For co-expression/co-immunoprecipitation studies, cells were lysed for 30 minutes on ice in
526 non-denaturing lysis buffer (NDLB) containing 50 mM HEPES pH 7.4, 150 mM NaCl, 1%
527 Triton X-100, 0.5% sodium deoxycholate, 25 mM β-glycerophosphate, 1 mM EDTA, 1 mM
528 EGTA, 1 mM Na3VO4, 1 μg mL^{-1} pepstatin, 2 μg mL^{-1} leupeptin, 2 μg mL^{-1} aprotinin, and 10
529 μM bestatin. Lysates were clarified at 12,000g for 10 minutes and pre-cleared with Protein
530 A/G agarose beads for 1 hour at 4°C. 5% of the lysates were set aside as input material and
531 the remainder was immunoprecipitated with appropriate antibodies for 0.5-4 hours at 4°C.
532 Protein A/G agarose beads blocked with 0.5% BSA were added in the final 30 minutes of
533 immunoprecipitation. Beads were then washed three times in NDLB and once in NDLB
534 containing 500 mM NaCl. For endogenous immunoprecipitation of ZNF165, ~$2x10^8$ cells
535 were collected and lysed in a hypotonic buffer (5 mM PIPES pH 8, 85 mM KCl, 0.5% NP-40)
536 supplemented with Complete Protease Inhibitor Cocktail (Sigma) for 20 minutes. Nuclei were
537 pelleted at 2,000 rpm for 5 minutes and resuspended in RIPA buffer (50 mM HEPES pH 7.4,
538 150 mM NaCl, 1% Triton X-100, 0.5% sodium deoxycholate, 0.5% SDS, 25 mM β-
539 glycerophosphate, 1 mM EDTA, 1 mM EGTA, 1 mM Na3VO4) supplemented with Complete
540 Protease Inhibitor Cocktail. Nuclear lysis was facilitated by gentle agitation at 4°C with

541 intermittent sonication (5-10 pulses at 5 seconds each). Lysates were clarified at 16,000g for
542 10 minutes, concentrated to a volume of 1-2 mL, and pre-cleared with Protein A/G agarose
543 beads for 1 hour at 4°C. 5% of the lysates were set aside as input material and the
544 remainder was subjected to immunoprecipitation overnight at 4°C. The next day, Protein A/G
545 agarose beads blocked with BSA were added to lysates for 2 hours, followed by four washes
546 in a buffer containing 50 mM HEPES pH 7.4, 150 mM NaCl, 1% Triton X-100, 25 mM β-
547 glycerophosphate, 1 mM EDTA, 1 mM EGTA, 1 mM Na3VO4, and Complete Protease
548 Inhibitor Cocktail. Immunoprecipitated proteins were eluted in 2X Laemmli sample buffer
549 (containing 4% β-mercaptoethanol) by boiling for 5-10 minutes.
550
551 **Soft agar assays**
552 4 X 10^3 SUM159 or MCF7 cells were trypsinized, counted, and resuspended in 0.366%
553 Bacto agar in complete medium and seeded on a layer of solidified 0.5% Bacto agar in 6-
554 well plates 48 hours post-transfection. After solidification, another layer of complete medium
555 containing 2X FBS was added. Cells were grown for 14 days (fed every 3 days) and then
556 stained with 0.05% crystal violet in phosphate-buffered saline (PBS) overnight. Images were
557 taken using a LEICA MZ75 stereomicroscope at a magnification of 6.3X and colony number
558 was quantified using ImageJ software.
559
560 **Tumor expression and patient survival analysis**
561 Normal/tumor expression data for ZNF446 and TRIM27 was generated by the TCGA
562 Research Network (https://www.cancer.gov/tcga) and visualized with Oncomine and
563 UALCAN, respectively (Rhodes et al. 2004; Chandrashekar et al. 2017). Survival analysis
564 was performed using Kaplan Meier plotter (Gyorffy et al. 2010). For ZNF165, expression
565 data was bifurcated using the upper quartile. For RRAD expression data was bifurcated
566 using median and lower tertile for OS and DMFS, respectively. For ZNF446, expression was
567 based on median values. Hazard ratios and p-values were calculated using the logrank test.

568

569 **Human breast tissue immunohistochemistry (IHC)**

570 Normal breast and TNBC tissues were obtained with informed consent from the UTSW
571 Tissue Management Shared Resource (TMSR) in compliance with the UTSW Internal
572 Review Board committee. TRIM27 IHC was optimized and performed by the TMSR
573 according to internal protocols using the Dako Autostainer Link 48 system. Quantification of
574 nuclear TRIM27 signal was performed using IHC Profiler (ImageJ) according to the
575 developer's guidelines (Varghese et al. 2014).

576

577 **Orthotopic xenografts**

578 SUM159T-Luciferase cells ($5x10^5$) stably expressing TRIM27 shRNAs or a non-targeting
579 hairpin were injected in the mammary fat pad of 10-week old female NOD.Cg-*Prkdc*^{scid}
580 *Il2rg*^{tm1Wjl}/SzJ (NSG) mice obtained from the Jackson Laboratory as previously described
581 (Westcott et al. 2015). Ten mice per condition were tested. Eight mice allowed for the
582 comparison of the mean values of two different samples (Control and Test) with a standard
583 deviation value of up to 60% of the difference between the means and a power of 0.8 using
584 a Two−sample t test. 10 mice were used to account for possible technical problems in handling
585 samples after the mouse is sacrificed, the need to prematurely sacrifice mice because of an adverse
586 response to surgical or non−surgical procedures or illness or complete failure of tumor growth.
587 Mice were assigned to groups randomly. Tumors were measured weekly using a digital
588 caliper and volume (V) was calculated using the following formula: $V = (Length \times (Width^2))/2$.
589 Starting four weeks post injection, tumors were measured weekly with bioluminescent
590 imaging (BLI). At six weeks post injection, mice were sacrificed after obtaining final BLI
591 measurements. These studies were conducted in accordance with a UT Southwestern
592 Institutional Animal Care and Use Committee (IACUC) approved protocol.

593

594 **Statistical analysis**

595 Graphpad Prism (Graphpad Software) was used to perform statistical analyses. Data were
596 assessed by one or two-tailed, unpaired t-tests or Mann-Whitney, or hypergeometric
597 distribution. P-values less than 0.05 were considered significant. Biological replicates were
598 considered to be experiments performed on distinct samples, while technical replicates were
599 considered identical samples run in parallel.
600

601 **ACKNOWLEDGEMENT**

602 We thank the Center for Cancer Systems Biology (CCSB) at the Dana-Farber Cancer
603 Institute for providing access to the human protein interactome database, and Melanie Cobb
604 and Michael Kalwat for comments and suggestions related to this study. We would also like
605 to acknowledge the assistance of the UTSW Tissue Management Shared Resource and the
606 UTSW Small Animal Imaging Resource, which are supported in part by the Harold C.
607 Simmons Cancer Center through an NCI Cancer Center Support Grant (5P30CA142543).
608 This work was supported by a donation from the families of Todd and Dawn Aaron and
609 Steven L. and Carol Aaron.
610

611 **REFERENCES**

612 Albagli O, Dhordain P, Deweindt C, Lecocq G, Leprince D. 1995. The BTB/POZ domain: a
613 new protein-protein interaction motif common to DNA- and actin-binding proteins.
614 *Cell Growth Differ* **6**: 1193-1198.
615 Asiedu MK, Ingle JN, Behrens MD, Radisky DC, Knutson KL. 2011. TGFbeta/TNF(alpha)-
616 mediated epithelial-mesenchymal transition generates breast cancer stem cells with
617 a claudin-low phenotype. *Cancer Res* **71**: 4707-4719.
618 Atanackovic D, Arfsten J, Cao Y, Gnjatic S, Schnieders F, Bartels K, Schilling G, Faltz C,
619 Wolschke C, Dierlamm J et al. 2007. Cancer-testis antigens are commonly
620 expressed in multiple myeloma and induce systemic immunity following allogeneic
621 stem cell transplantation. *Blood* **109**: 1103-1112.
622 Bardwell VJ, Treisman R. 1994. The POZ domain: a conserved protein-protein interaction
623 motif. *Genes Dev* **8**: 1664-1677.
624 Bellefroid EJ, Poncelet DA, Lecocq PJ, Revelant O, Martial JA. 1991. The evolutionarily
625 conserved Kruppel-associated box domain defines a subfamily of eukaryotic
626 multifingered proteins. *Proc Natl Acad Sci U S A* **88**: 3608-3612.
627 Bhola NE, Balko JM, Dugger TC, Kuba MG, Sanchez V, Sanders M, Stanford J, Cook RS,
628 Arteaga CL. 2013. TGF-beta inhibition enhances chemotherapy action against triple-
629 negative breast cancer. *J Clin Invest* **123**: 1348-1358.

630 Cappell KM, Sinnott R, Taus P, Maxfield K, Scarbrough M, Whitehurst AW. 2012. Multiple
631 cancer testis antigens function to support tumor cell mitotic fidelity. *Mol Cell Biol* **32**:
632 4131-4140.
633 Challen GA, Boles NC, Chambers SM, Goodell MA. 2010. Distinct hematopoietic stem cell
634 subtypes are differentially regulated by TGF-beta1. *Cell Stem Cell* **6**: 265-278.
635 Chandrashekar DS, Bashel B, Balasubramanya SAH, Creighton CJ, Ponce-Rodriguez I,
636 Chakravarthi B, Varambally S. 2017. UALCAN: A Portal for Facilitating Tumor
637 Subgroup Gene Expression and Survival Analyses. *Neoplasia* **19**: 649-658.
638 Chang L, Zhang J, Tseng YH, Xie CQ, Ilany J, Bruning JC, Sun Z, Zhu X, Cui T, Youker KA
639 et al. 2007. Rad GTPase deficiency leads to cardiac hypertrophy. *Circulation* **116**:
640 2976-2983.
641 Chen CR, Kang Y, Siegel PM, Massague J. 2002. E2F4/5 and p107 as Smad cofactors
642 linking the TGFbeta receptor to c-myc repression. *Cell* **110**: 19-32.
643 Chen W, Schwalie PC, Pankevich EV, Gubelmann C, Raghav SK, Dainese R, Cassano M,
644 Imbeault M, Jang SM, Russeil J et al. 2019. ZFP30 promotes adipogenesis through
645 the KAP1-mediated activation of a retrotransposon-derived Pparg2 enhancer. *Nat*
646 *Commun* **10**: 1809.
647 Chen YT, Scanlan MJ, Sahin U, Tureci O, Gure AO, Tsang S, Williamson B, Stockert E,
648 Pfreundschuh M, Old LJ. 1997. A testicular antigen aberrantly expressed in human
649 cancers detected by autologous antibody screening. *Proc Natl Acad Sci U S A* **94**:
650 1914-1918.
651 Chu Y, Yang X. 2011. SUMO E3 ligase activity of TRIM proteins. *Oncogene* **30**: 1108-1116.
652 Edelstein LC, Collins T. 2005. The SCAN domain family of zinc finger transcription factors.
653 *Gene* **359**: 1-17.
654 Feng XH, Zhang Y, Wu RY, Derynck R. 1998. The tumor suppressor Smad4/DPC4 and
655 transcriptional adaptor CBP/p300 are coactivators for smad3 in TGF-beta-induced
656 transcriptional activation. *Genes Dev* **12**: 2153-2163.
657 Fijak M, Meinhardt A. 2006. The testis in immune privilege. *Immunol Rev* **213**: 66-81.
658 Friedman JR, Fredericks WJ, Jensen DE, Speicher DW, Huang XP, Neilson EG, Rauscher
659 FJ, 3rd. 1996. KAP-1, a novel corepressor for the highly conserved KRAB repression
660 domain. *Genes Dev* **10**: 2067-2078.
661 Gallegos ZR, Taus P, Gibbs ZA, McGlynn K, Gomez NC, Davis I, Whitehurst AW. 2019.
662 EWSR1-FLI1 Activation of the Cancer/Testis Antigen FATE1 Promotes Ewing
663 Sarcoma Survival. *Mol Cell Biol* **39**.
664 Gibbs ZA, Whitehurst AW. 2018. Emerging Contributions of Cancer/Testis Antigens to
665 Neoplastic Behaviors. *Trends Cancer* **4**: 701-712.
666 Gomis RR, Alarcon C, He W, Wang Q, Seoane J, Lash A, Massague J. 2006. A FoxO-Smad
667 synexpression group in human keratinocytes. *Proc Natl Acad Sci U S A* **103**: 12747-
668 12752.
669 Goumans MJ, Valdimarsdottir G, Itoh S, Rosendahl A, Sideras P, ten Dijke P. 2002.
670 Balancing the activation state of the endothelium via two distinct TGF-beta type I
671 receptors. *EMBO J* **21**: 1743-1753.
672 Gyorffy B, Lanczky A, Eklund AC, Denkert C, Budczies J, Li Q, Szallasi Z. 2010. An online
673 survival analysis tool to rapidly assess the effect of 22,277 genes on breast cancer
674 prognosis using microarray data of 1,809 patients. *Breast Cancer Res Treat* **123**:
675 725-731.
676 Hannon GJ, Beach D. 1994. p15INK4B is a potential effector of TGF-beta-induced cell cycle
677 arrest. *Nature* **371**: 257-261.
678 Hao YH, Doyle JM, Ramanathan S, Gomez TS, Jia D, Xu M, Chen ZJ, Billadeau DD, Rosen
679 MK, Potts PR. 2013. Regulation of WASH-dependent actin polymerization and
680 protein trafficking by ubiquitination. *Cell* **152**: 1051-1064.
681 Horio M, Kato T, Mii S, Enomoto A, Asai M, Asai N, Murakumo Y, Shibata K, Kikkawa F,
682 Takahashi M. 2012. Expression of RET finger protein predicts chemoresistance in
683 epithelial ovarian cancer. *Cancer Med* **1**: 218-229.

684 Hosoya N, Okajima M, Kinomura A, Fujii Y, Hiyama T, Sun J, Tashiro S, Miyagawa K. 2011.
685 Synaptonemal complex protein SYCP3 impairs mitotic recombination by interfering
686 with BRCA2. *EMBO Rep* **13**: 44-51.
687 Hsiao BY, Chang TK, Wu IT, Chen MY. 2014. Rad GTPase inhibits the NFkappaB pathway
688 through interacting with RelA/p65 to impede its DNA binding and target gene
689 transactivation. *Cell Signal* **26**: 1437-1444.
690 Inman GJ, Nicolas FJ, Callahan JF, Harling JD, Gaster LM, Reith AD, Laping NJ, Hill CS.
691 2002. SB-431542 is a potent and specific inhibitor of transforming growth factor-beta
692 superfamily type I activin receptor-like kinase (ALK) receptors ALK4, ALK5, and
693 ALK7. *Mol Pharmacol* **62**: 65-74.
694 Iwakoshi A, Murakumo Y, Kato T, Kitamura A, Mii S, Saito S, Yatabe Y, Takahashi M. 2012.
695 RET finger protein expression is associated with prognosis in lung cancer with
696 epidermal growth factor receptor mutations. *Pathol Int* **62**: 324-330.
697 Janknecht R, Wells NJ, Hunter T. 1998. TGF-beta-stimulated cooperation of smad proteins
698 with the coactivators CBP/p300. *Genes Dev* **12**: 2114-2119.
699 Lambert SA, Jolma A, Campitelli LF, Das PK, Yin Y, Albu M, Chen X, Taipale J, Hughes TR,
700 Weirauch MT. 2018. The Human Transcription Factors. *Cell* **172**: 650-665.
701 Lee I, Yeom SY, Lee SJ, Kang WK, Park C. 2010. A novel senescence-evasion mechanism
702 involving Grap2 and Cyclin D interacting protein inactivation by Ras associated with
703 diabetes in cancer cells under doxorubicin treatment. *Cancer Res* **70**: 4357-4365.
704 Lee JT, Shan J, Zhong J, Li M, Zhou B, Zhou A, Parsons R, Gu W. 2013. RFP-mediated
705 ubiquitination of PTEN modulates its effect on AKT activation. *Cell Res* **23**: 552-564.
706 Lehmann BD, Bauer JA, Chen X, Sanders ME, Chakravarthy AB, Shyr Y, Pietenpol JA.
707 2011. Identification of human triple-negative breast cancer subtypes and preclinical
708 models for selection of targeted therapies. *J Clin Invest* **121**: 2750-2767.
709 Li S, Shen D, Shao J, Crowder R, Liu W, Prat A, He X, Liu S, Hoog J, Lu C et al. 2013.
710 Endocrine-therapy-resistant ESR1 variants revealed by genomic characterization of
711 breast-cancer-derived xenografts. *Cell Rep* **4**: 1116-1130.
712 Li TF, O'Keefe RJ, Chen D. 2005. TGF-beta signaling in chondrocytes. *Front Biosci* **10**: 681-
713 688.
714 Liu F, Zhu C, Xiao J, Wang Y, Tang W, Yuan W, Zhao Y, Li Y, Xiang Z, Wu X et al. 2005. A
715 novel human KRAB-containing zinc-finger gene ZNF446 inhibits transcriptional
716 activities of SRE and AP-1. *Biochem Biophys Res Commun* **333**: 5-13.
717 Liu J, Zhang C, Wu R, Lin M, Liang Y, Liu J, Wang X, Yang B, Feng Z. 2015. RRAD inhibits
718 the Warburg effect through negative regulation of the NF-kappaB signaling.
719 *Oncotarget* **6**: 14982-14992.
720 Ma Y, Wei Z, Bast RC, Jr., Wang Z, Li Y, Gao M, Liu Y, Wang X, Guo C, Zhang L et al.
721 2016. Downregulation of TRIM27 expression inhibits the proliferation of ovarian
722 cancer cells in vitro and in vivo. *Lab Invest* **96**: 37-48.
723 Manning JR, Yin G, Kaminski CN, Magyar J, Feng HZ, Penn J, Sievert G, Thompson K, Jin
724 JP, Andres DA et al. 2013. Rad GTPase deletion increases L-type calcium channel
725 current leading to increased cardiac contraction. *J Am Heart Assoc* **2**: e000459.
726 Martin-Malpartida P, Batet M, Kaczmarska Z, Freier R, Gomes T, Aragon E, Zou Y, Wang Q,
727 Xi Q, Ruiz L et al. 2017. Structural basis for genome wide recognition of 5-bp GC
728 motifs by SMAD transcription factors. *Nat Commun* **8**: 2070.
729 Massague J. 2008. TGFbeta in Cancer. *Cell* **134**: 215-230.
730 -. 2012. TGFbeta signalling in context. *Nat Rev Mol Cell Biol* **13**: 616-630.
731 Maxfield KE, Taus PJ, Corcoran K, Wooten J, Macion J, Zhou Y, Borromeo M, Kollipara RK,
732 Yan J, Xie Y et al. 2015. Comprehensive functional characterization of cancer-testis
733 antigens defines obligate participation in multiple hallmarks of cancer. *Nat Commun*
734 **6**: 8840.
735 Meza U, Beqollari D, Romberg CF, Papadopoulos S, Bannister RA. 2013. Potent inhibition
736 of L-type Ca2+ currents by a Rad variant associated with congestive heart failure.
737 *Biochem Biophys Res Commun* **439**: 270-274.

738 Mo Y, Midorikawa K, Zhang Z, Zhou X, Ma N, Huang G, Hiraku Y, Oikawa S, Murata M.
739 2012. Promoter hypermethylation of Ras-related GTPase gene RRAD inactivates a
740 tumor suppressor function in nasopharyngeal carcinoma. *Cancer Lett* **323**: 147-154.
741 Morikawa M, Derynck R, Miyazono K. 2016. TGF-beta and the TGF-beta Family: Context-
742 Dependent Roles in Cell and Tissue Physiology. *Cold Spring Harb Perspect Biol* **8**.
743 Mullen AC, Orlando DA, Newman JJ, Loven J, Kumar RM, Bilodeau S, Reddy J, Guenther
744 MG, DeKoter RP, Young RA. 2011. Master transcription factors determine cell-type-
745 specific responses to TGF-beta signaling. *Cell* **147**: 565-576.
746 Nichols BA, Oswald NW, McMillan EA, McGlynn K, Yan J, Kim MS, Saha J, Mallipeddi PL,
747 LaDuke SA, Villalobos PA et al. 2018. HORMAD1 Is a Negative Prognostic Indicator
748 in Lung Adenocarcinoma and Specifies Resistance to Oxidative and Genotoxic
749 Stress. *Cancer Res* **78**: 6196-6208.
750 Padua D, Zhang XH, Wang Q, Nadal C, Gerald WL, Gomis RR, Massague J. 2008.
751 TGFbeta primes breast tumors for lung metastasis seeding through angiopoietin-like
752 4. *Cell* **133**: 66-77.
753 Perou CM, Sorlie T, Eisen MB, van de Rijn M, Jeffrey SS, Rees CA, Pollack JR, Ross DT,
754 Johnsen H, Akslen LA et al. 2000. Molecular portraits of human breast tumours.
755 *Nature* **406**: 747-752.
756 Petersen M, Pardali E, van der Horst G, Cheung H, van den Hoogen C, van der Pluijm G,
757 Ten Dijke P. 2010. Smad2 and Smad3 have opposing roles in breast cancer bone
758 metastasis by differentially affecting tumor angiogenesis. *Oncogene* **29**: 1351-1361.
759 Pineda CT, Ramanathan S, Fon Tacer K, Weon JL, Potts MB, Ou YH, White MA, Potts PR.
760 2015. Degradation of AMPK by a cancer-specific ubiquitin ligase. *Cell* **160**: 715-728.
761 Polyak K, Kato JY, Solomon MJ, Sherr CJ, Massague J, Roberts JM, Koff A. 1994. p27Kip1,
762 a cyclin-Cdk inhibitor, links transforming growth factor-beta and contact inhibition to
763 cell cycle arrest. *Genes Dev* **8**: 9-22.
764 Prat A, Parker JS, Karginova O, Fan C, Livasy C, Herschkowitz JI, He X, Perou CM. 2010.
765 Phenotypic and molecular characterization of the claudin-low intrinsic subtype of
766 breast cancer. *Breast Cancer Res* **12**: R68.
767 Rhodes DR, Yu J, Shanker K, Deshpande N, Varambally R, Ghosh D, Barrette T, Pandey A,
768 Chinnaiyan AM. 2004. ONCOMINE: a cancer microarray database and integrated
769 data-mining platform. *Neoplasia* **6**: 1-6.
770 Robinson JT, Thorvaldsdottir H, Winckler W, Guttman M, Lander ES, Getz G, Mesirov JP.
771 2011. Integrative genomics viewer. *Nat Biotechnol* **29**: 24-26.
772 Rolland T, Tasan M, Charloteaux B, Pevzner SJ, Zhong Q, Sahni N, Yi S, Lemmens I,
773 Fontanillo C, Mosca R et al. 2014. A proteome-scale map of the human interactome
774 network. *Cell* **159**: 1212-1226.
775 Sabatier R, Finetti P, Guille A, Adelaide J, Chaffanet M, Viens P, Birnbaum D, Bertucci F.
776 2014. Claudin-low breast cancers: clinical, pathological, molecular and prognostic
777 characterization. *Mol Cancer* **13**: 228.
778 Sahin U, Koslowski M, Tureci O, Eberle T, Zwick C, Romeike B, Moringlane JR,
779 Schwechheimer K, Feiden W, Pfreundschuh M. 2000. Expression of cancer testis
780 genes in human brain tumors. *Clin Cancer Res* **6**: 3916-3922.
781 Sahin U, Tureci O, Schmitt H, Cochlovius B, Johannes T, Schmits R, Stenner F, Luo G,
782 Schobert I, Pfreundschuh M. 1995. Human neoplasms elicit multiple specific immune
783 responses in the autologous host. *Proc Natl Acad Sci U S A* **92**: 11810-11813.
784 Sato M, Kadota M, Tang B, Yang HH, Yang YA, Shan M, Weng J, Welsh MA, Flanders KC,
785 Nagano Y et al. 2014. An integrated genomic approach identifies persistent tumor
786 suppressive effects of transforming growth factor-beta in human breast cancer.
787 *Breast Cancer Res* **16**: R57.
788 Schultz DC, Ayyanathan K, Negorev D, Maul GG, Rauscher FJ, 3rd. 2002. SETDB1: a novel
789 KAP-1-associated histone H3, lysine 9-specific methyltransferase that contributes to
790 HP1-mediated silencing of euchromatic genes by KRAB zinc-finger proteins. *Genes*
791 *Dev* **16**: 919-932.

792 Schultz DC, Friedman JR, Rauscher FJ, 3rd. 2001. Targeting histone deacetylase
793 complexes via KRAB-zinc finger proteins: the PHD and bromodomains of KAP-1
794 form a cooperative unit that recruits a novel isoform of the Mi-2alpha subunit of
795 NuRD. *Genes Dev* **15**: 428-443.
796 Shang R, Wang J, Sun W, Dai B, Ruan B, Zhang Z, Yang X, Gao Y, Qu S, Lv X et al. 2016.
797 RRAD inhibits aerobic glycolysis, invasion, and migration and is associated with poor
798 prognosis in hepatocellular carcinoma. *Tumour Biol* **37**: 5097-5105.
799 Shimono Y, Murakami H, Hasegawa Y, Takahashi M. 2000. RET finger protein is a
800 transcriptional repressor and interacts with enhancer of polycomb that has dual
801 transcriptional functions. *J Biol Chem* **275**: 39411-39419.
802 Shimono Y, Murakami H, Kawai K, Wade PA, Shimokata K, Takahashi M. 2003. Mi-2 beta
803 associates with BRG1 and RET finger protein at the distinct regions with
804 transcriptional activating and repressing abilities. *J Biol Chem* **278**: 51638-51645.
805 Simpson AJ, Caballero OL, Jungbluth A, Chen YT, Old LJ. 2005. Cancer/testis antigens,
806 gametogenesis and cancer. *Nat Rev Cancer* **5**: 615-625.
807 Sorlie T, Perou CM, Tibshirani R, Aas T, Geisler S, Johnsen H, Hastie T, Eisen MB, van de
808 Rijn M, Jeffrey SS et al. 2001. Gene expression patterns of breast carcinomas
809 distinguish tumor subclasses with clinical implications. *Proc Natl Acad Sci U S A* **98**:
810 10869-10874.
811 Suzuki M, Shigematsu H, Shames DS, Sunaga N, Takahashi T, Shivapurkar N, Iizasa T,
812 Minna JD, Fujisawa T, Gazdar AF. 2007. Methylation and gene silencing of the Ras-
813 related GTPase gene in lung and breast cancers. *Ann Surg Oncol* **14**: 1397-1404.
814 Takahashi M, Ritz J, Cooper GM. 1985. Activation of a novel human transforming gene, ret,
815 by DNA rearrangement. *Cell* **42**: 581-588.
816 Tezel G, Nagasaka T, Iwahashi N, Asai N, Iwashita T, Sakata K, Takahashi M. 1999.
817 Different nuclear/cytoplasmic distributions of RET finger protein in different cell types.
818 *Pathol Int* **49**: 881-886.
819 Tezel GG, Uner A, Yildiz I, Guler G, Takahashi M. 2009. RET finger protein expression in
820 invasive breast carcinoma: relationship between RFP and ErbB2 expression. *Pathol*
821 *Res Pract* **205**: 403-408.
822 Thomas R, Al-Khadairi G, Roelands J, Hendrickx W, Dermime S, Bedognetti D, Decock J.
823 2018. NY-ESO-1 Based Immunotherapy of Cancer: Current Perspectives. *Front*
824 *Immunol* **9**: 947.
825 Tian F, DaCosta Byfield S, Parks WT, Yoo S, Felici A, Tang B, Piek E, Wakefield LM,
826 Roberts AB. 2003. Reduction in Smad2/3 signaling enhances tumorigenesis but
827 suppresses metastasis of breast cancer cell lines. *Cancer Res* **63**: 8284-8292.
828 Tirosvoutis KN, Divane A, Jones M, Affara NA. 1995. Characterization of a novel zinc finger
829 gene (ZNF165) mapping to 6p21 that is expressed specifically in testis. *Genomics*
830 **28**: 485-490.
831 Tseng YH, Vicent D, Zhu J, Niu Y, Adeyinka A, Moyers JS, Watson PH, Kahn CR. 2001.
832 Regulation of growth and tumorigenicity of breast cancer cells by the low molecular
833 weight GTPase Rad and nm23. *Cancer Res* **61**: 2071-2079.
834 Tsukamoto H, Kato T, Enomoto A, Nakamura N, Shimono Y, Jijiwa M, Asai N, Murakumo Y,
835 Shibata K, Kikkawa F et al. 2009. Expression of Ret finger protein correlates with
836 outcomes in endometrial cancer. *Cancer Sci* **100**: 1895-1901.
837 Tufegdzic Vidakovic A, Rueda OM, Vervoort SJ, Sati Batra A, Goldgraben MA, Uribe-Lewis
838 S, Greenwood W, Coffer PJ, Bruna A, Caldas C. 2015. Context-Specific Effects of
839 TGF-beta/SMAD3 in Cancer Are Modulated by the Epigenome. *Cell Rep* **13**: 2480-
840 2490.
841 Uhlen M, Fagerberg L, Hallstrom BM, Lindskog C, Oksvold P, Mardinoglu A, Sivertsson A,
842 Kampf C, Sjostedt E, Asplund A et al. 2015. Proteomics. Tissue-based map of the
843 human proteome. *Science* **347**: 1260419.

844 van der Bruggen P, Traversari C, Chomez P, Lurquin C, De Plaen E, Van den Eynde B,
845 Knuth A, Boon T. 1991. A gene encoding an antigen recognized by cytolytic T
846 lymphocytes on a human melanoma. *Science* **254**: 1643-1647.
847 Varghese F, Bukhari AB, Malhotra R, De A. 2014. IHC Profiler: an open source plugin for the
848 quantitative evaluation and automated scoring of immunohistochemistry images of
849 human tissue samples. *PLoS One* **9**: e96801.
850 Viphakone N, Cumberbatch MG, Livingstone MJ, Heath PR, Dickman MJ, Catto JW, Wilson
851 SA. 2015. Luzp4 defines a new mRNA export pathway in cancer cells. *Nucleic Acids*
852 *Res* **43**: 2353-2366.
853 Wang C, Gu Y, Zhang K, Xie K, Zhu M, Dai N, Jiang Y, Guo X, Liu M, Dai J et al. 2016.
854 Systematic identification of genes with a cancer-testis expression pattern in 19
855 cancer types. *Nat Commun* **7**: 10499.
856 Westcott JM, Prechtl AM, Maine EA, Dang TT, Esparza MA, Sun H, Zhou Y, Xie Y, Pearson
857 GW. 2015. An epigenetically distinct breast cancer cell subpopulation promotes
858 collective invasion. *J Clin Invest* **125**: 1927-1943.
859 Whitehurst AW. 2014. Cause and consequence of cancer/testis antigen activation in cancer.
860 *Annu Rev Pharmacol Toxicol* **54**: 251-272.
861 Whitehurst AW, Xie Y, Purinton SC, Cappell KM, Swanik JT, Larson B, Girard L, Schorge
862 JO, White MA. 2010. Tumor antigen acrosin binding protein normalizes mitotic
863 spindle function to promote cancer cell proliferation. *Cancer Res* **70**: 7652-7661.
864 Williams AJ, Khachigian LM, Shows T, Collins T. 1995. Isolation and characterization of a
865 novel zinc-finger protein with transcription repressor activity. *J Biol Chem* **270**:
866 22143-22152.
867 Xu J, Lamouille S, Derynck R. 2009. TGF-beta-induced epithelial to mesenchymal transition.
868 *Cell Res* **19**: 156-172.
869 Yeom SY, Lee SJ, Kim WS, Park C. 2012. Rad knockdown induces mitochondrial apoptosis
870 in bortezomib resistant leukemia and lymphoma cells. *Leuk Res* **36**: 1172-1178.
871 Zaman MM, Nomura T, Takagi T, Okamura T, Jin W, Shinagawa T, Tanaka Y, Ishii S. 2013.
872 Ubiquitination-deubiquitination by the TRIM27-USP7 complex regulates tumor
873 necrosis factor alpha-induced apoptosis. *Mol Cell Biol* **33**: 4971-4984.
874 Zha J, Han KJ, Xu LG, He W, Zhou Q, Chen D, Zhai Z, Shu HB. 2006. The Ret finger protein
875 inhibits signaling mediated by the noncanonical and canonical IkappaB kinase family
876 members. *J Immunol* **176**: 1072-1080.
877 Zhang C, Liu J, Wu R, Liang Y, Lin M, Liu J, Chan CS, Hu W, Feng Z. 2014. Tumor
878 suppressor p53 negatively regulates glycolysis stimulated by hypoxia through its
879 target RRAD. *Oncotarget* **5**: 5535-5546.
880 Zhang Y, Feng Y, Ji D, Wang Q, Qian W, Wang S, Zhang Z, Ji B, Zhang C, Sun Y et al.
881 2018. TRIM27 functions as an oncogene by activating epithelial-mesenchymal
882 transition and p-AKT in colorectal cancer. *Int J Oncol* **53**: 620-632.
883 Zheng Q, Hou J, Zhou Y, Yang Y, Xie B, Cao X. 2015. Siglec1 suppresses antiviral innate
884 immune response by inducing TBK1 degradation via the ubiquitin ligase TRIM27.
885 *Cell Res* **25**: 1121-1136.
886 Zoumpoulidou G, Broceno C, Li H, Bird D, Thomas G, Mittnacht S. 2012. Role of the
887 tripartite motif protein 27 in cancer development. *J Natl Cancer Inst* **104**: 941-952.
888 Zurek B, Schoultz I, Neerincx A, Napolitano LM, Birkner K, Bennek E, Sellge G, Lerm M,
889 Meroni G, Soderholm JD et al. 2012. TRIM27 negatively regulates NOD2 by
890 ubiquitination and proteasomal degradation. *PLoS One* **7**: e41255.

891

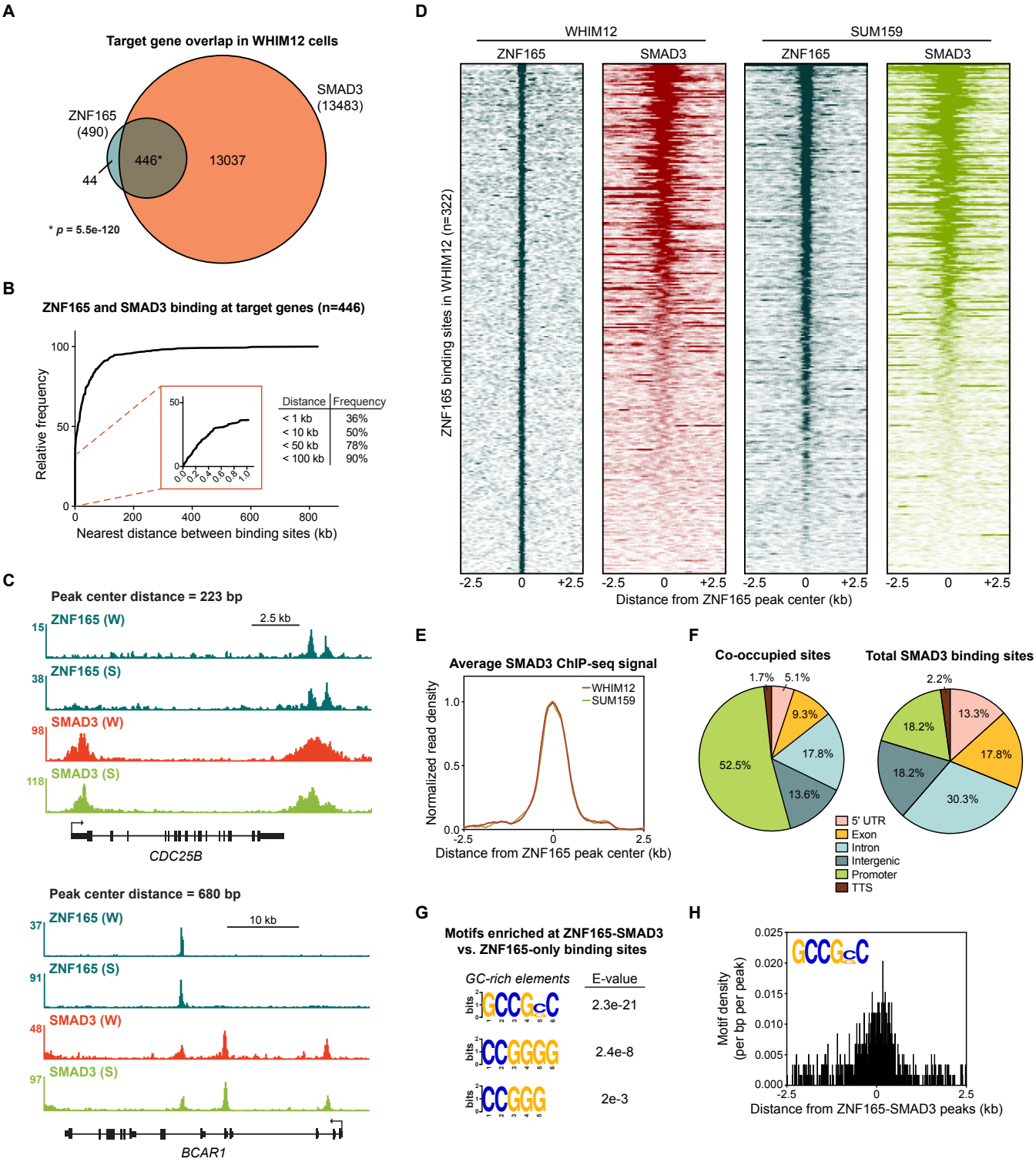

Figure 1. SMAD3 is enriched at ZNF165 binding sites in TNBC cells. (**A**) Venn diagram displaying the overlap between ZNF165 and SMAD3 target genes in WHIM12 cells as identified by GREAT (ver 3.0.0). Significance was determined using the hypergeometric distribution. (**B**) Cumulative frequency distribution of the nearest distance between ZNF165 and SMAD3 binding sites associated with each shared target gene. Distance was calculated using the peak coordinates of each factor nearest to one another. (**C**) Browser tracks of ChIP-seq data showing peaks for ZNF165 and SMAD3 near the *CDC25B* and *BCAR1* loci with overlapping distances of 223 and 680 bp, respectively. (W) WHIM12, (S) SUM159. (**D**) Heatmaps of ChIP-seq data for ZNF165 and SMAD3 in the indicated TNBC cell lines. All peaks within each heatmap are centered ± 2.5 kb from the ZNF165 peaks identified in WHIM12 cells (n=322). (**E**) Normalized read density (per bp per peak) for SMAD3 plotted ± 2.5 kb from the ZNF165-SMAD3 co-bound peaks identified in WHIM12 cells (n=118). (**F**) Pie charts displaying the distribution of genomic features bound by ZNF165-SMAD3 or only SMAD3 in WHIM12 cells. (**G**) Motifs enriched at ZNF165-SMAD3 co-bound sites within WHIM12 cells. The 204 ZNF165 binding sites not occupied by SMAD3 were used as a control set of sequences to identify differentially enriched motifs at the shared sites (n=118). (**H**) Motif density (per bp per peak) for the GCCG(G|C)C motif plotted ± 2.5 kb from the centers of ZNF165-SMAD3 co-bound peaks in WHIM12 cells.

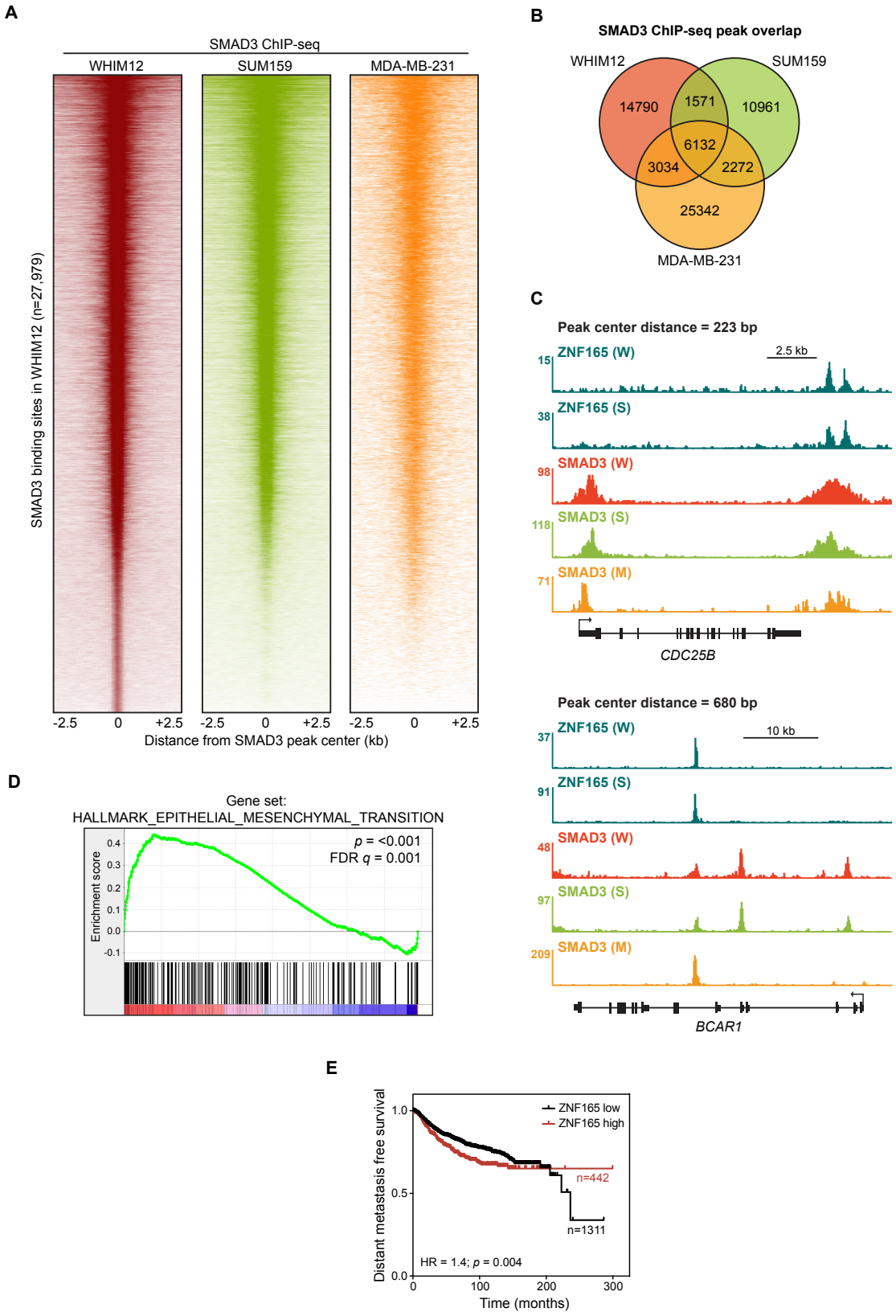

Figure 1-figure supplement 1. SMAD3 is enriched at ZNF165 binding sites in TNBC cells. (**A**) Heatmaps of SMAD3 ChIP-seq data in WHIM12, SUM159, and MDA-MB-231 cells. All peaks within each heatmap are centered ± 2.5 kb from the SMAD3 peaks identified in WHIM12 cells (n=27,979). Data for MDA-MB-231 cells were obtained from EGAS00001001570 (Tufegdzic Vidakovic et al. 2015). (**B**) Venn diagram displaying the overlap between SMAD3 peaks identified in each cell line. (**C**) Browser tracks of ChIP-seq data showing peaks for ZNF165 and SMAD3 near the *CDC25B* and *BCAR1* loci with overlapping distances of 223 and 680 bp, respectively. (W) WHIM12, (S) SUM159, (M) MDA-MB-231. (**D**) Gene set enrichment analysis (GSEA) of ZNF165-responsive genes in WHIM12 cells. Transcriptome data for ZNF165 knockdown was obtained from GSE63984 (Maxfield et al. 2015). (**E**) Kaplan-Meier plot displaying distant metastasis free survival in breast cancer patients with high or low ZNF165 expression. P-value and hazard ratio (HR) were calculated using the logrank test.

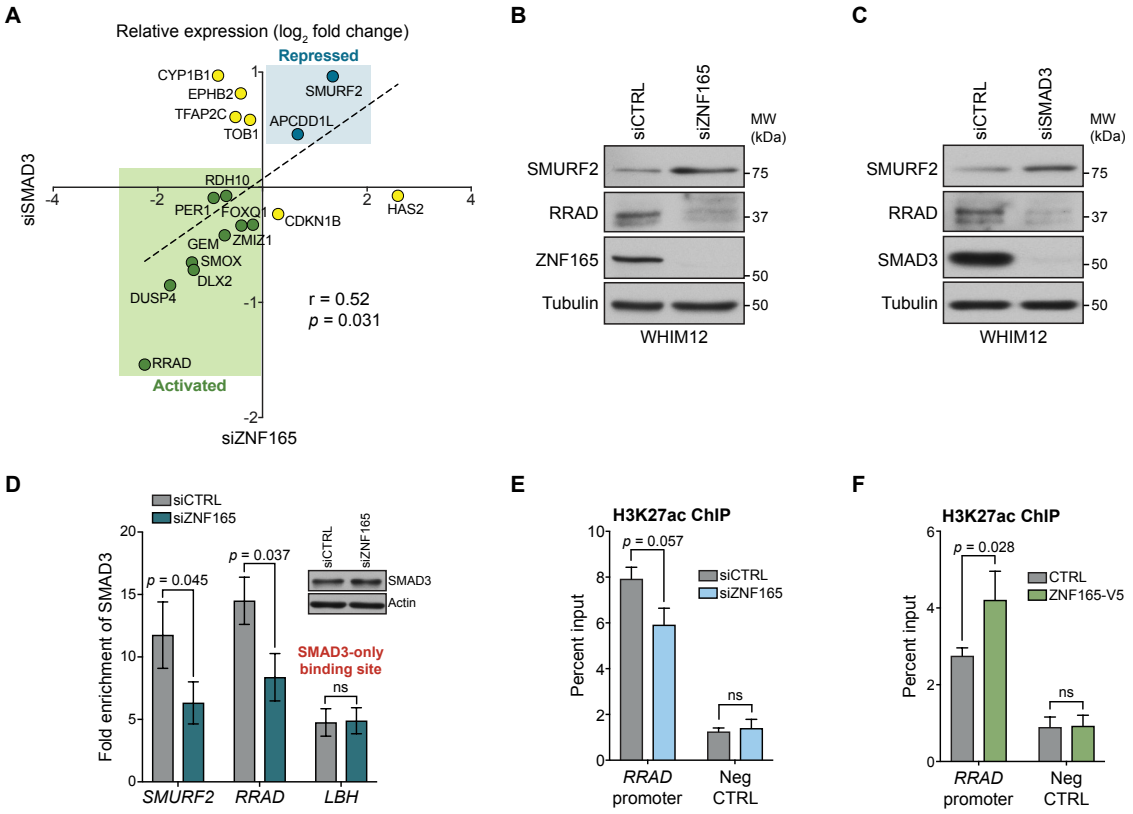

Figure 2. ZNF165 and SMAD3 cooperate to modulate TGFβ-responsive gene expression. (**A**) WHIM12 cells were transfected with siRNA for 48h, and qPCR was used to quantify relative expression ($\log_2$ fold change) of ZNF165-SMAD3 target genes upon depletion of ZNF165 (x-axis) or SMAD3 (y-axis). The Pearson correlation coefficient is indicated by r. Data are representative of four independent experiments. (**B**) WHIM12 cells were transfected with siRNA for 72h. Whole cell lysates were collected and immunoblotted for the indicated proteins. Data are representative of two independent experiments. (**C**) As in (B) except cells were transfected with siRNA targeting SMAD3. (**D**) SUM159 cells were transfected with siRNA for 32h and subjected to SMAD3 ChIP followed by qPCR using primers targeting the indicated binding sites. Fold enrichment was determined by dividing the percent input values for SMAD3 by those for IgG. Error bars represent mean ± SEM. P-values were calculated using an unpaired, two-tailed Student's t-test. Data are representative of four independent experiments. (**E**) SUM159 cells were transfected with siRNA for 32h and subjected to H3K27ac ChIP followed by qPCR using primers targeted to the RRAD promoter or a negative control region. Error bars represent mean + SEM. P-value was calculated using an unpaired, two-tailed Mann-Whitney test. Data are representative of four independent experiments. (**F**) SUM159 cells stably expressing ZNF165-V5 or control cDNA were subjected to H3K27ac ChIP followed by qPCR using primers targeted to the RRAD promoter or a negative control region. Error bars represent mean + SEM. P-value was calculated using an unpaired, two-tailed Mann-Whitney test. Data are representative of four independent experiments.

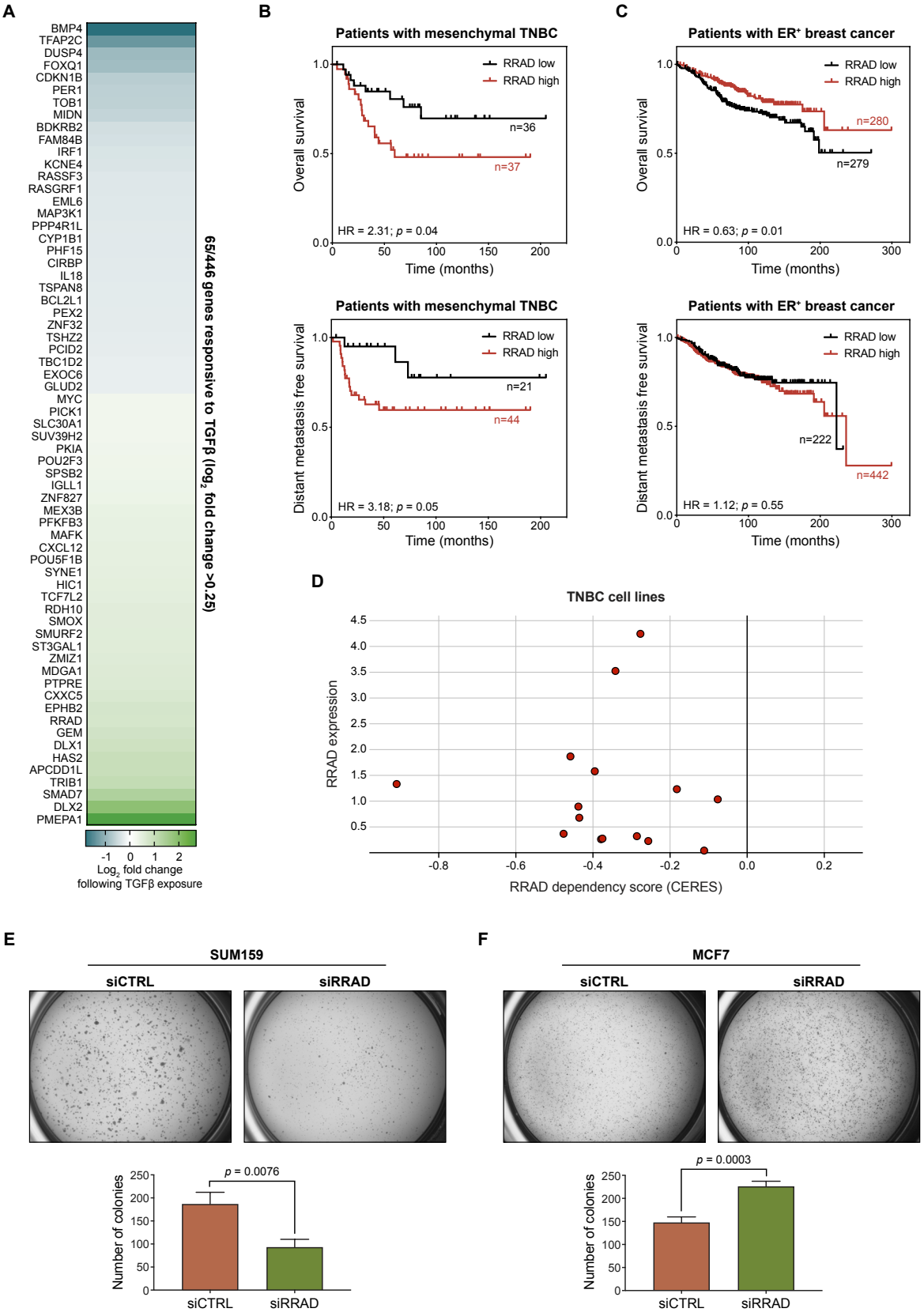
A
BMP4
TFAP2C
DUSP4
FOXQ1
CDKN1B
PER1
TOB1
MIDN
BDKRB2
FAM84B
IRF1
KCNE4
RASSF3
RASGRF1
EML6
MAP3K1
PPP4R1L
CYP1B1
PHF15
CIRBP
IL18
TSPAN8
BCL2L1
PEX2
ZNF32
TSHZ2
PCID2
TBC1D2
EXOC6
GLUD2
MYC
PICK1
SLC30A1
SUV39H2
PKIA
POU2F3
SPSB2
IGLL1
ZNF827
MEX3B
PFKFB3
MAFK
CXCL12
POU5F1B
SYNE1
HIC1
TCF7L2
RDH10
SMOX
SMURF2
ST3GAL1
ZMIZ1
MDGA1
PTPRE
CXXC5
EPHB2
RRAD
GEM
DLX1
HAS2
APCDD1L
TRIB1
SMAD7
DLX2
PMEPA1
65/446 genes responsive to TGFβ (log2 fold change >0.25)
-1 0 1 2
Log2 fold change following TGFβ exposure
B
Patients with mesenchymal TNBC
RRAD low
RRAD high
n=36
n=37
HR = 2.31; p = 0.04
Overall survival
Time (months)
Patients with mesenchymal TNBC
n=21
n=44
HR = 3.18; p = 0.05
Distant metastasis free survival
Time (months)
C
Patients with ER+ breast cancer
n=280
n=279
HR = 0.63; p = 0.01
Overall survival
Time (months)
Patients with ER+ breast cancer
n=222
n=442
HR = 1.12; p = 0.55
Distant metastasis free survival
Time (months)
D
TNBC cell lines
RRAD expression
RRAD dependency score (CERES)
E
SUM159
siCTRL
siRRAD
p = 0.0076
Number of colonies
siCTRL
siRRAD
F
MCF7
siCTRL
siRRAD
p = 0.0003
Number of colonies
siCTRL
siRRAD

Figure 2-figure supplement 1. ZNF165 and SMAD3 activate *RRAD* to drive neoplastic behaviors in TNBC. (**A**) Heatmap plotting the $\log_2$ fold-change in expression of 65/446 shared ZNF165-SMAD3 target genes (cutoff > 0.25) following TGFβ exposure in WHIM12 cells. Expression data were obtained from GSE63986 (Maxfield et al. 2015). (**B**) Kaplan-Meier plots displaying overall survival and distant metastasis free survival (DMFS) for patients with the mesenchymal subtype of TNBC and high or low RRAD expression. P-values and hazard ratios (HRs) were calculated using the logrank test. (**C**) As in (B) except for patients with ER^+ breast cancer. (**D**) TNBC cell line dependency scores calculated from CRISPR-mediated perturbation (as determined by CERES) plotted against RRAD expression (log2(TPM+1)) (Barretina et al. 2012; Meyers et al. 2017). Negative dependency scores represent a decrease in viability. Data were obtained from the Cancer Dependency Map (depmap.org). (**E**) Soft agar growth assays for SUM159 cells transfected with indicated siRNAs. Error bars represent mean + SEM. P-value was calculated using an unpaired, two-tailed Student's t-test. Data are representative of three independent experiments. (**F**) As in (E) except using MCF7 cells.

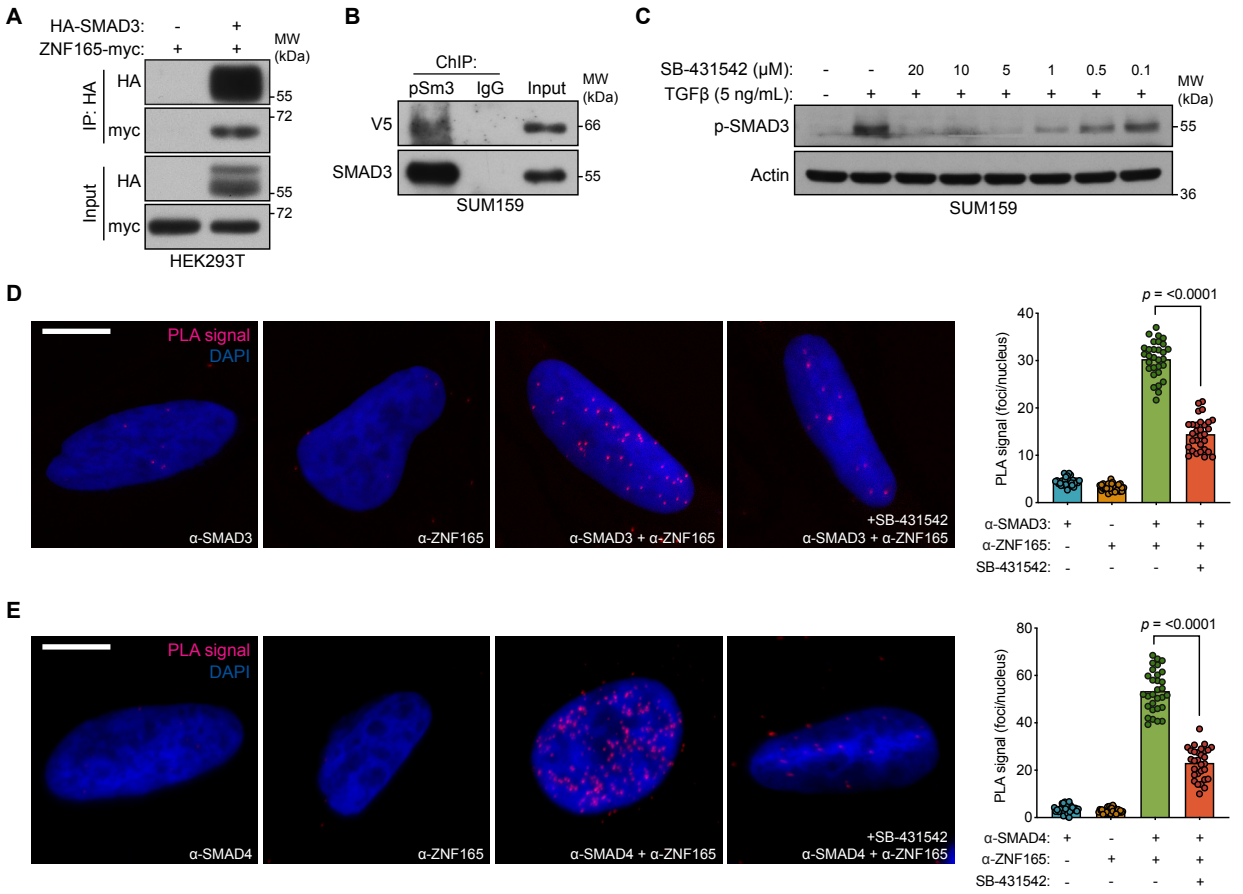

Figure 3. ZNF165 physically associates with SMAD3 in a TGFβ-dependent manner. (**A**) Forty-eight hours after transfection with HA-SMAD3 and/or ZNF165-myc cDNA, HEK293T cells were subjected to immunoprecipitation with HA antibody. Immunoblotting was performed with indicated antibodies. Data are representative of two independent experiments. (**B**) ChIP was performed in SUM159 cells with antibodies against phosphorylated SMAD3 (Ser423/425) or IgG, and the precipitated material was immunoblotted with indicated antibodies. Data are representative of two independent experiments. (**C**) SUM159 cells were pre-treated with SB-431542 at the indicated concentrations for 15 minutes, followed by stimulation with 5 ng mL^{-1} TGFβ for 30 minutes. Immunoblotting was performed with indicated antibodies. Data are representative of two independent experiments. (**D**) Proximity ligation assays (PLAs) performed using antibodies against endogenous ZNF165 and SMAD3 in SUM159 cells, where either antibody alone was used as a negative control. Cells were pre-treated with 20 μM SB-431542 or DMSO for 15 minutes, followed by stimulation with 5 ng mL^{-1} TGFβ for 30 minutes. Scale bars, 10 μm. The mean PLA signal (number of foci per nucleus) is quantified (right), where each data point represents the mean signal calculated within one image. P-value was calculated using an unpaired, two-tailed Student's t-test. Ten images were used per condition and data are representative of three independent assays. (**E**) As in (D) except antibodies against endogenous ZNF165 and SMAD4 were used.

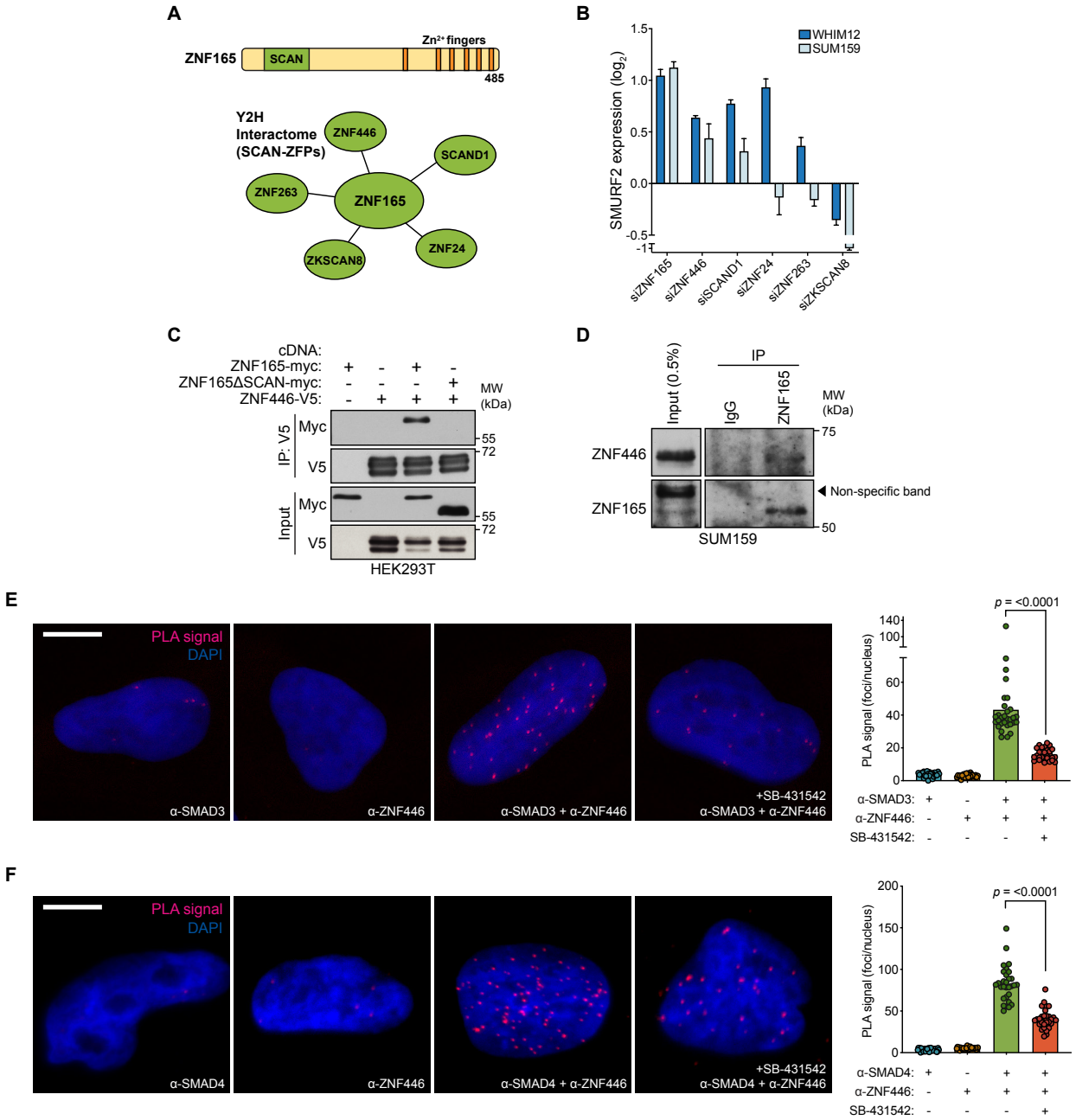

Figure 4. ZNF446 is an obligate component of the ZNF165-SMAD3 transcriptional complex. (**A**) ZNF165 interactors that contain a SCAN domain as identified from a systematic yeast two-hybrid screening approach (interactome.dfci.harvard.edu). A domain map of ZNF165 is shown above for reference. (**B**) Forty-eight hours after transfection with indicated siRNAs, RNA was extracted from WHIM12 or SUM159 cells and qPCR was used to determine the relative expression of SMURF2. Log_2 fold-change values normalized to control knockdown samples are displayed. Error bars represent mean + SEM. P-values were calculated for each sample using a one-tailed Mann-Whitney test. Data are representative of three independent experiments. (**C**) Forty-eight hours after transfection with indicated cDNA, HEK293T lysates were subjected to immunoprecipitation with V5 antibody. Immunoblotting was performed with indicated antibodies. Data are representative of three independent experiments. (**D**) SUM159 nuclear lysates were immunoprecipated with antibodies against endogenous ZNF165 or IgG. Immunoblotting was performed with indicated antibodies. (**E**) Proximity ligation assays (PLAs) performed using antibodies against endogenous ZNF446 and SMAD3 in SUM159 cells, where either antibody alone was used as a negative control. Cells were pre-treated with 20 μM SB-431542 or DMSO for 15 minutes, followed by stimulation with 5 ng mL^{-1} TGFβ for 30 minutes. Scale bars, 10 μm. The mean PLA signal (number of foci per nucleus) is quantified (right), where each data point represents the mean signal calculated within one image. P-value was calculated using an unpaired, two-tailed Student's t-test. Ten images were used per condition and data are representative of three independent assays. (**F**) As in (E) except antibodies against endogenous ZNF446 and SMAD4 were used.

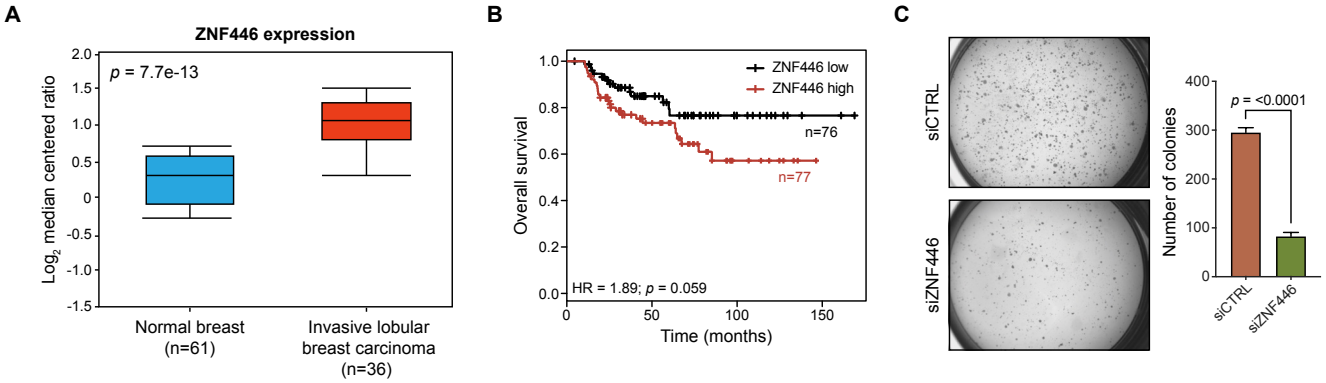

Figure 4-figure supplement 1. ZNF446 expression is elevated in breast cancer and associated with poor prognosis. (**A**) Box-plot showing ZNF446 expression values (log_2 median centered ratio) from normal breast and invasive lobular breast carcinoma. Data were obtained from TCGA and p-value was calculated using an unpaired, two-tailed Student's t-test. (**B**) Kaplan-Meier plot displaying overall survival of patients with the basal-like subtype of breast cancer and either low or high ZNF446 expression. P-value and hazard ratio (HR) were calculated using the logrank test. (**C**) Soft agar growth assays for SUM159 cells transfected with indicated siRNAs. Error bars represent mean + SEM. P-value was calculated using an unpaired, two-tailed Student's t-test. Data are representative of three independent experiments.

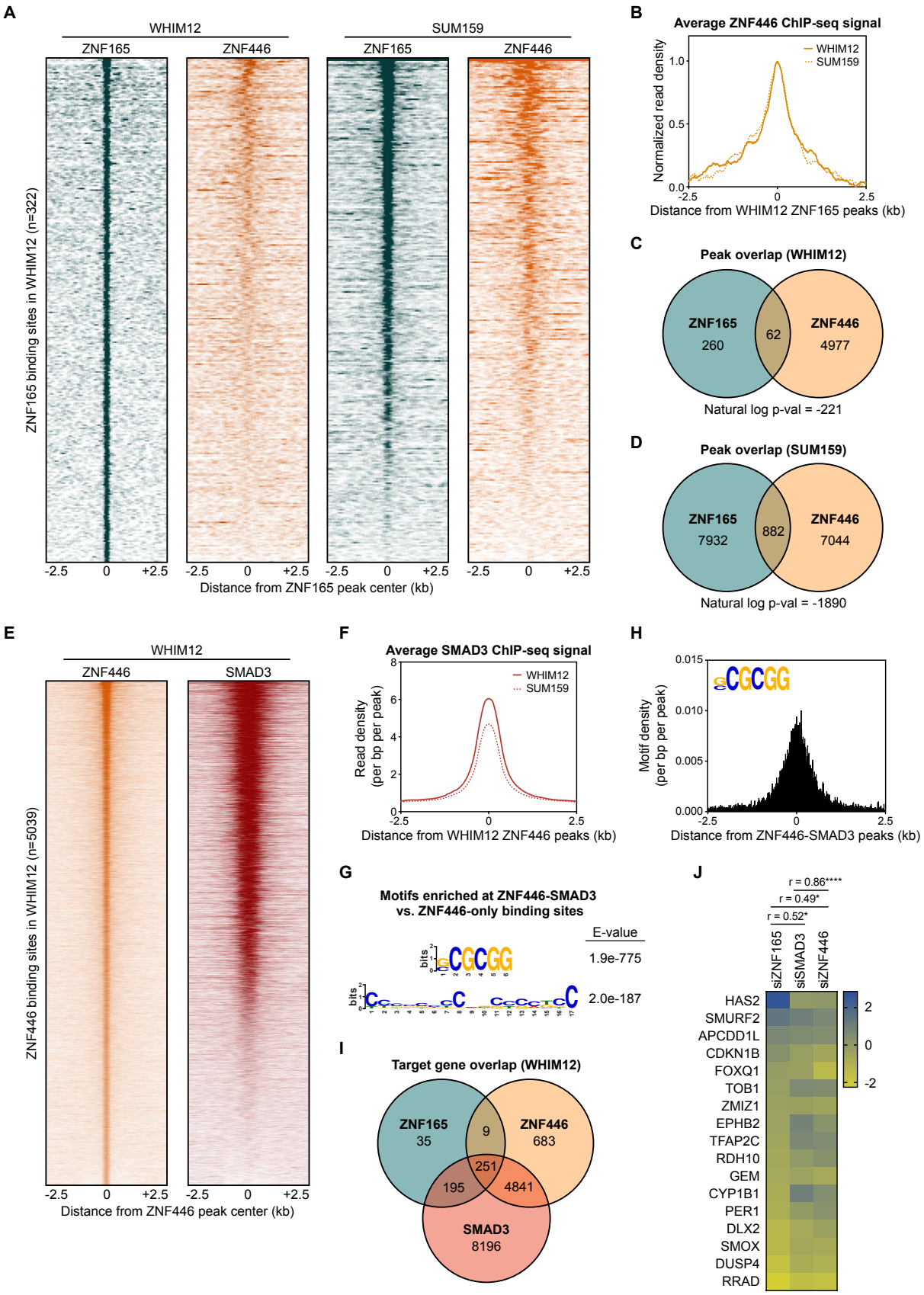
A
WHIM12
SUM159
ZNF165
ZNF446
ZNF165
ZNF446
ZNF165 binding sites in WHIM12 (n=322)
-2.5
0
+2.5
Distance from ZNF165 peak center (kb)
B
Average ZNF446 ChIP-seq signal
WHIM12
SUM159
Normalized read density
1.0
0.5
0.0
-2.5
0
2.5
Distance from WHIM12 ZNF165 peaks (kb)
C
Peak overlap (WHIM12)
ZNF165
260
62
ZNF446
4977
Natural log p-val = -221
D
Peak overlap (SUM159)
ZNF165
7932
882
ZNF446
7044
Natural log p-val = -1890
E
WHIM12
ZNF446
SMAD3
ZNF446 binding sites in WHIM12 (n=5039)
-2.5
0
+2.5
Distance from ZNF446 peak center (kb)
F
Average SMAD3 ChIP-seq signal
WHIM12
SUM159
Read density
(per bp per peak)
8
6
4
2
0
-2.5
0
2.5
Distance from WHIM12 ZNF446 peaks (kb)
H
Motif density
(per bp per peak)
0.015
0.010
0.005
0.000
-2.5
0
2.5
Distance from ZNF446-SMAD3 peaks (kb)
G
Motifs enriched at ZNF446-SMAD3
vs. ZNF446-only binding sites
E-value
1.9e-775
2.0e-187
bits
I
Target gene overlap (WHIM12)
ZNF165
35
9
ZNF446
683
251
195
4841
SMAD3
8196
J
r = 0.86****
r = 0.49*
r = 0.52*
siZNF165
siSMAD3
siZNF446
HAS2
SMURF2
APCDD1L
CDKN1B
FOXQ1
TOB1
ZMIZ1
EPHB2
TFAP2C
RDH10
GEM
CYP1B1
PER1
DLX2
SMOX
DUSP4
RRAD
2
0
-2

Figure 5. ZNF446 co-occupies a subset of both ZNF165 and SMAD3 binding sites in TNBC cells. (**A**) Heatmaps of ChIP-seq data for ZNF165 and ZNF446 in the indicated TNBC cell lines. All peaks within each heatmap are centered ± 2.5 kb from the WHIM12 ZNF165 peaks (n=322). (**B**) Normalized read density (per bp per peak) for ZNF446 plotted ± 2.5 kb from the ZNF165 peaks identified in WHIM12 cells (n=322). (**C**) Peak overlap between ZNF165 and ZNF446 in WHIM12 cells. P-value was calculated using the hypergeometric distribution. (**D**) As in (C) except using peaks identified for ZNF165 and ZNF446 in SUM159 cells. (**E**) Heatmaps of ChIP-seq data for ZNF446 and SMAD3 in WHIM12 cells. All peaks within each heatmap are centered ± 2.5 kb from the ZNF446 peaks (n=5,039). (**F**) Read density (per bp per peak) for SMAD3 plotted ± 2.5 kb from the ZNF446 peaks identified in WHIM12 cells (n=5,039). (**G**) Motifs enriched at ZNF446-SMAD3 co-bound sites within WHIM12 cells. The ZNF446 binding sites not occupied by SMAD3 (n=2,587) were used as a control set of sequences to identify differentially enriched motifs at the shared sites (n=2,376). (**H**) Motif density (per bp per peak) for the (G|C)CGCGG motif plotted ± 2.5 kb from the centers of ZNF446-SMAD3 co-bound peaks in WHIM12 cells. (**I**) Venn diagram displaying the overlap between ZNF165, SMAD3, and ZNF446 target genes from WHIM12 cells as identified by GREAT (ver 3.0.0). (**J**) Heatmap displaying $\log_2$ fold-changes of ZNF165-SMAD3 targets in response to depletion of ZNF446, as well as either ZNF165 or SMAD3. The Pearson correlation coefficient is indicated by r. Significance is indicated by asterisks, where * = $p < 0.05$ and **** = $p < 0.0001$. Data are representative of four independent experiments.

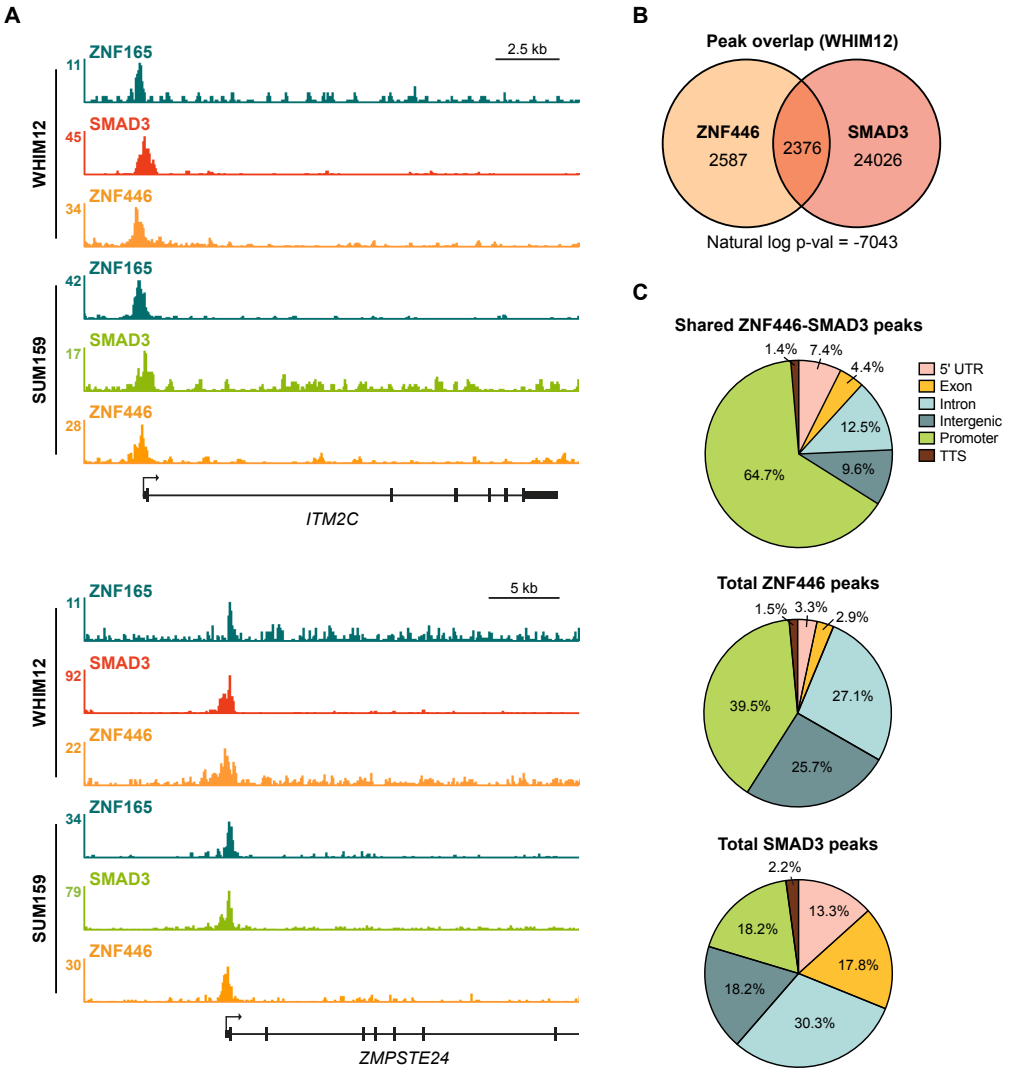

Figure 5-figure supplement 1. ZNF446 co-occupies a subset of both ZNF165 and SMAD3 binding sites in TNBC cells. (**A**) Browser tracks of ChIP-seq data showing peaks for ZNF165, SMAD3, and ZNF446 near the *ITM2C* and *ZMPSTE24* loci in WHIM12 or SUM159 cells. (**B**) Peak overlap between ZNF446 and SMAD3 in WHIM12 cells. P-value was calculated using the hypergeometric distribution. (**C**) Pie charts displaying the distribution of genomic features bound by ZNF446-SMAD3 or either transcription factor alone in WHIM12 cells.

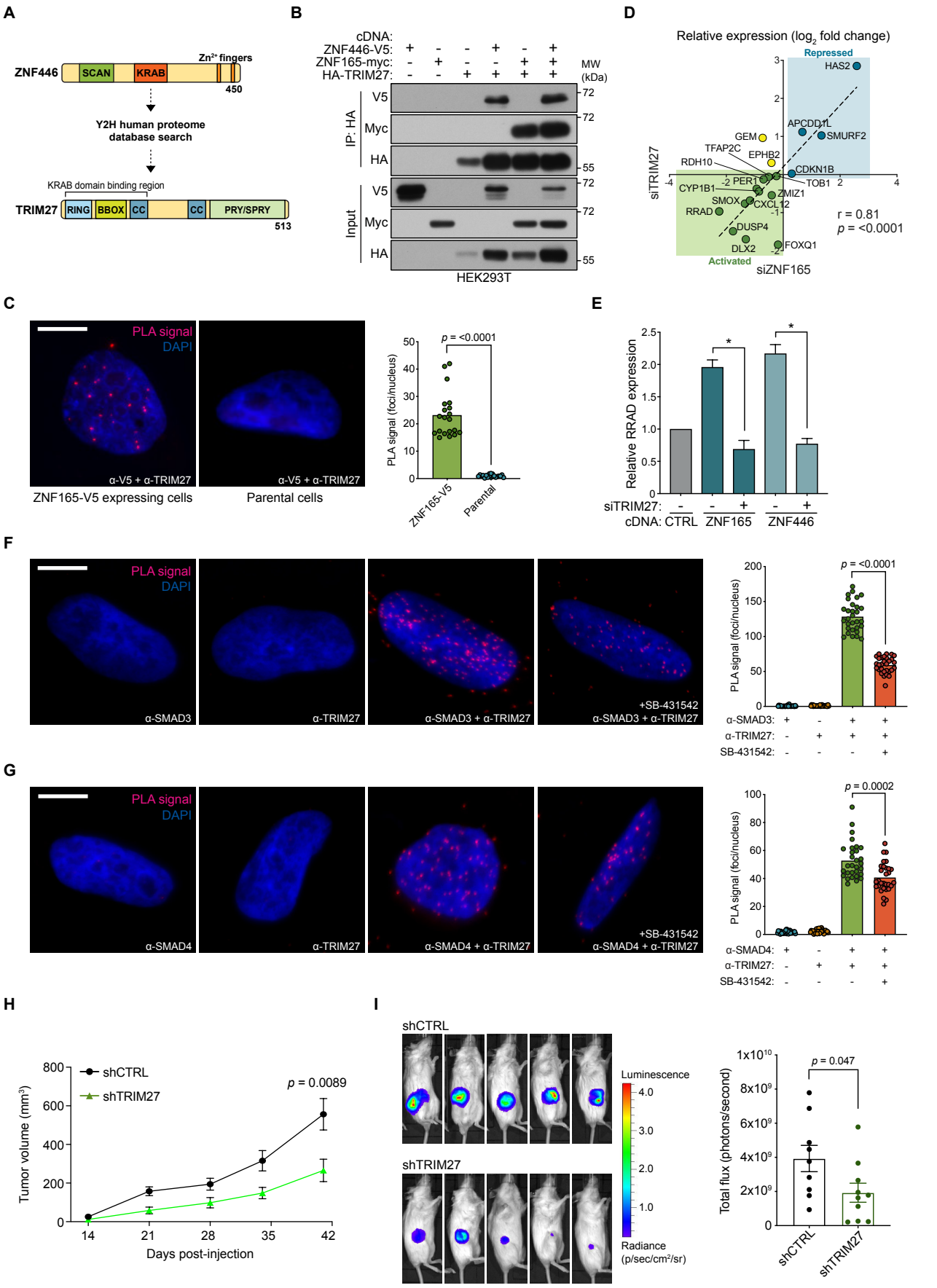
A
ZNF446
SCAN
KRAB
Zn2+ fingers
450
Y2H human proteome database search
KRAB domain binding region
TRIM27
RING
BBOX
CC
CC
PRY/SPRY
513
B
cDNA:
ZNF446-V5:
ZNF165-myc:
HA-TRIM27:
MW (kDa)
IP: HA
V5
Myc
HA
Input
V5
Myc
HA
72
72
55
72
72
55
HEK293T
D
Relative expression (log2 fold change)
Repressed
Activated
HAS2
APCDD1L
SMURF2
GEM
TFAP2C
EPHB2
RDH10
CDKN1B
TOB1
PER1
CYP1B1
ZMIZ1
SMOX
CXCL12
RRAD
DUSP4
DLX2
FOXQ1
siTRIM27
siZNF165
r = 0.81
p = <0.0001
C
PLA signal
DAPI
α-V5 + α-TRIM27
α-V5 + α-TRIM27
ZNF165-V5 expressing cells
Parental cells
p = <0.0001
PLA signal (foci/nucleus)
ZNF165-V5
Parental
E
Relative RRAD expression
siTRIM27:
cDNA: CTRL ZNF165 ZNF446
F
PLA signal
DAPI
α-SMAD3
α-TRIM27
α-SMAD3 + α-TRIM27
+SB-431542
α-SMAD3 + α-TRIM27
p = <0.0001
PLA signal (foci/nucleus)
α-SMAD3:
α-TRIM27:
SB-431542:
G
PLA signal
DAPI
α-SMAD4
α-TRIM27
α-SMAD4 + α-TRIM27
+SB-431542
α-SMAD4 + α-TRIM27
p = 0.0002
PLA signal (foci/nucleus)
α-SMAD4:
α-TRIM27:
SB-431542:
H
shCTRL
shTRIM27
p = 0.0089
Tumor volume (mm3)
Days post-injection
I
shCTRL
shTRIM27
Luminescence
Radiance (p/sec/cm2/sr)
p = 0.047
Total flux (photons/second)
shCTRL
shTRIM27

Figure 6. TRIM27 is essential for ZNF165 transcriptional activity and tumor growth *in vivo*. (**A**) Cartoon maps showing the domains of ZNF446 and TRIM27. The KRAB-binding domain of TRIM27 is highlighted for reference. (**B**) Forty-eight hours after transfection with indicated cDNA, HEK293T lysates were subjected to immunoprecipitation with HA antibody. Immunoblotting was performed using indicated antibodies. Data are representative of three independent experiments. (**C**) Proximity ligation assays (PLAs) performed using V5 and TRIM27 antibodies in SUM159 cells stably expressing ZNF165-V5. Parental SUM159 cells were used as a negative control with the V5/TRIM27 antibody combination. Scale bar, 10 µm. The mean PLA signal (number of foci per nucleus) is quantified (right), where each data point represents the mean signal calculated within one image. P-values were calculated using an unpaired, two-tailed Student's t-test. Five images were used per condition and data are representative of four independent assays. (**D**) WHIM12 cells were transfected with siRNA for 48h and qPCR was used to quantify relative expression (log_2 fold change) of shared ZNF165-SMAD3 target genes upon depletion of ZNF165 (x-axis) or TRIM27 (y-axis). The Pearson correlation coefficient is indicated by r. Data are representative of three independent experiments. (**E**) SUM159 cells stably expressing indicated cDNA were transfected with siRNA targeting TRIM27 for 48h. Relative RRAD expression was measured using qPCR and the data were normalized to the CTRL sample (grey). Error bars represent mean + SEM. P-values were calculated using an unpaired, two-tailed Mann-Whitney test. Significance is indicated by asterisks, where * = $p < 0.05$. Data are representative of four independent experiments. (**F**) PLAs performed using antibodies against endogenous TRIM27 and SMAD3 in SUM159 cells, where either antibody alone was used as a negative control. Cells were pre-treated with 20 µM SB-431542 or DMSO for 15 minutes, followed by stimulation with 5 ng mL^{-1} TGFβ for 30 minutes. Scale bar, 10 µm. The mean PLA signal (number of foci per nucleus) is quantified (right), where each data point represents the mean signal calculated within one image. P-value was calculated using an unpaired, two-tailed Student's t-test. Ten images were used per condition and data are representative of three independent assays. (**G**) As in (F) except antibodies against endogenous TRIM27 and SMAD4 were used. (**H**) Tumor volumes from mice orthotopically injected with SUM159T-Luciferase cells stably expressing shRNAs against TRIM27 (n=10) or a non-targeting control (n=9). P-value was calculated using an unpaired, two-tailed Student's t-test. (**I**) Representative images of bioluminescence (BLI) measurements taken for mice from each group. BLI data was quantified (right) and the p-value was calculated using an unpaired, two-tailed Student's t-test.

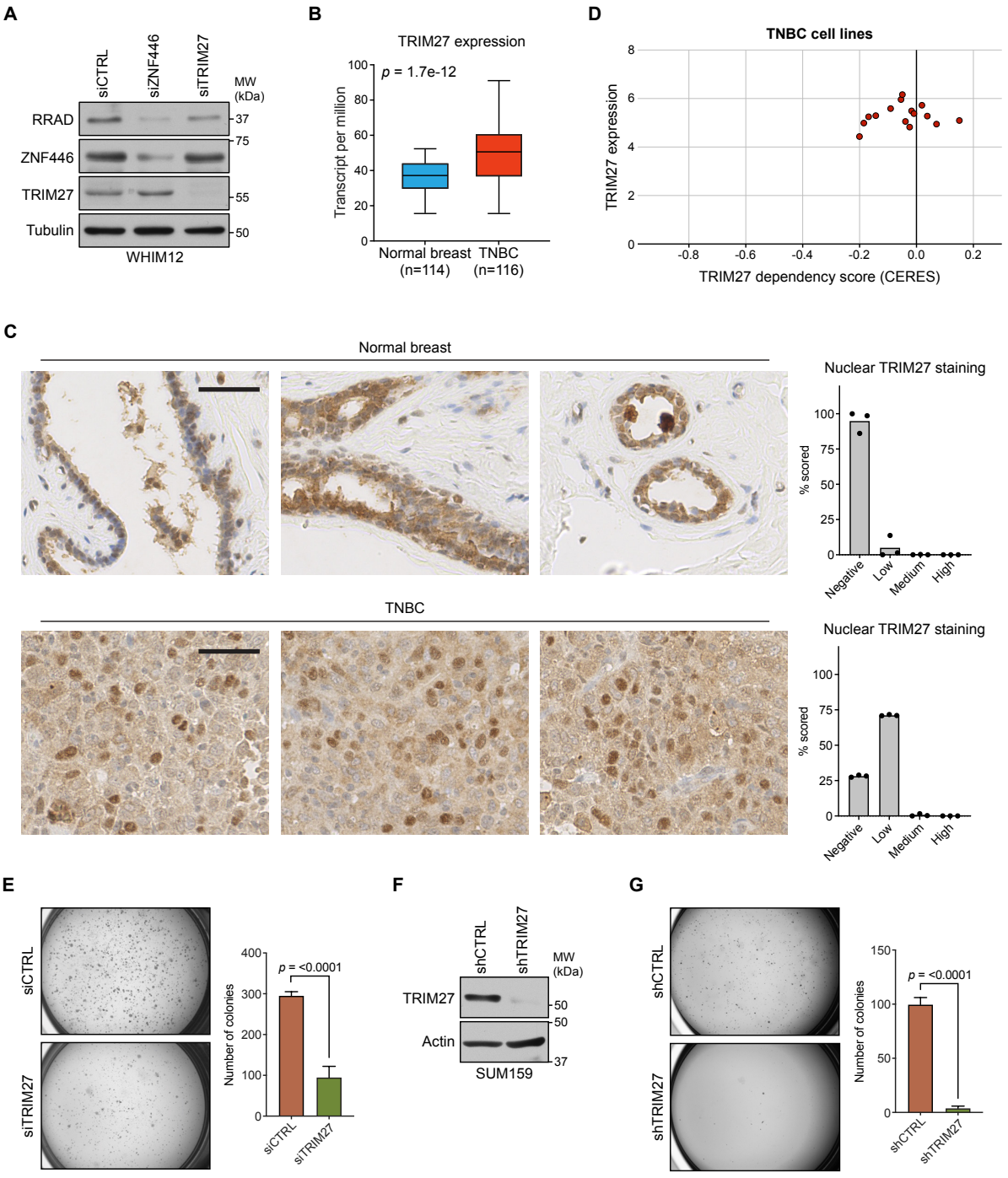

Figure 6-figure supplement 1. Analysis of TRIM27 expression and contribution to neoplastic behaviors in TNBC. (**A**) WHIM12 cells were transfected with indicated siRNA for 72h. Whole cell lysates were collected and immunoblotted for the indicated proteins. Data are representative of two independent experiments. (**B**) Box-plot showing TRIM27 expression values (transcript per million) from normal breast and TNBC. Data were obtained from TCGA and the p-value was calculated using an unpaired, two-tailed Student's t-test. (**C**) Immunohistochemistry (IHC) staining for TRIM27 in patient-derived normal breast and TNBC tissues. Scale bar, 50 μm. Nuclear staining was scored (right) using IHC Profiler (Varghese et al. 2014). (**D**) TNBC cell line dependency scores calculated from CRISPR-mediated perturbation (as determined by CERES) plotted against TRIM27 expression (log2(TPM+1)) (Barretina et al. 2012; Meyers et al. 2017). Negative or positive dependency scores represent a decrease or increase in viability, respectively. Data were obtained from the Cancer Dependency Map (depmap.org). (**E**) Soft agar growth assays for SUM159 cells transfected with indicated siRNAs. Error bars represent mean + SEM. P-value was calculated using an unpaired, two-tailed Student's t-test. Data are representative of three independent experiments. (**F**) SUM159T-Luciferase cells were transduced with indicated shRNAs. After 72h, whole cell lysates were collected and immunoblotted for the indicated proteins. Data are representative of two independent experiments. (**G**) Soft agar growth assays for SUM159T-Luciferase cells transduced with indicated shRNAs. Error bars represent mean + SEM. P-value was calculated using an unpaired, two-tailed Student's t-test. Data are representative of three independent experiments.

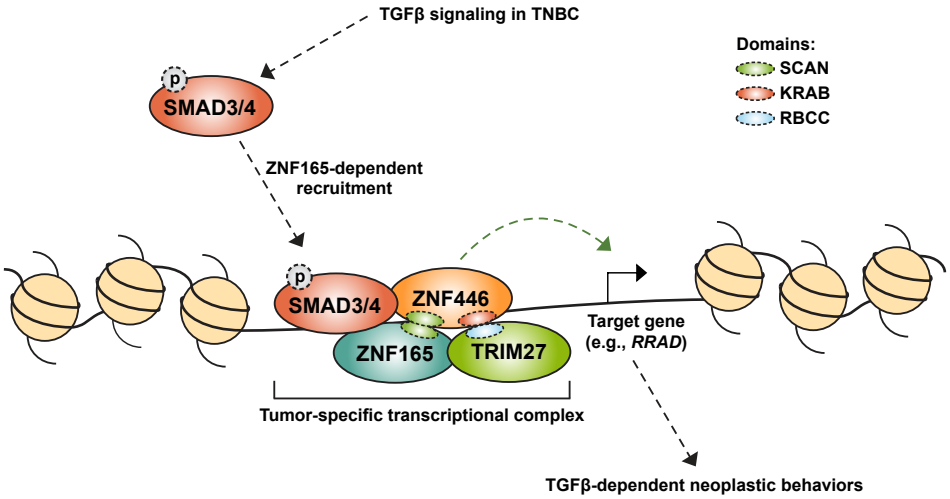

Figure 7. Model for assembly of a neomorphic ZNF165 transcriptional complex in TNBC. Aberrant expression of testis-specific ZNF165 in TNBC co-opts somatic transcriptional machinery to modulate TGFβ-dependent transcription. The ZNF165 SCAN domain recruits ZNF446, and together these factors associate with SMAD3 at shared binding sites throughout the genome and alter gene expression to promote neoplastic behaviors. Via its KRAB domain, ZNF446 recruits the co-activator/co-repressor TRIM27, which is essential for ZNF165 transcriptional activity and tumor growth *in vivo*. Given the testis/tumor-restricted expression of ZNF165, disruption of this complex holds potential as a therapeutic strategy to specifically inhibit pro-tumorigenic TGFβ signaling in TNBC.